Effect of Salinity and Hardness on Hydrolyzed Polyacrylamide Rheology in Sandstone

R. S. Seright[1]*, Stephane Jouenne[2], and Carl Aften[3]

[1]New Mexico Institute of Mining & Technology
[2]TotalEnergies
[3]SNF Holding Company

Summary

In this paper, we clarify the impact of salinity and hardness on partially hydrolyzed polyacrylamide (HPAM) rheology in sandstones with permeability greater than 200 md. For modelers/simulators of polymer flooding, the experimental findings should be of high relevance when projecting HPAM injectivity, fracture initiation, and whether viscoelasticity is significant in oil recovery of capillary-trapped residual oil with or without the presence of fractures. The literature review summarizes the effects of polymer concentration, molecular weight (Mw), rock permeability, and oil saturation on HPAM rheology in sandstones. The experimental work examines HPAM (18–20 million g/mol Mw, 30% degree of hydrolysis) rheology in sandstones with permeabilities ranging from 252 md to 838 md, salinities ranging from 0.1% to 10.5% total dissolved solids (TDS), and hardness levels ranging from 0% to 0.1% calcium chloride ($CaCl_2$). As expected, the magnitude of resistance factors increased with increased HPAM concentration but decreased with increased salinity. The maximum resistance factor in the shear-thickening regime correlated well with $C[\mu]/(k/\phi)^{0.5}$. The velocity dependence of the rheology (in sandstone) was largely unchanged by salinity between 0.1% and 5% TDS. At 1% TDS, the velocity dependence of rheology (in sandstone) was very weakly dependent on $CaCl_2$ concentration between 0% and 0.1%. We examine the relationship between the onset of shear thickening and the inverse of the polymer solution relaxation time determined from bulk rheological data. The level of mechanical degradation was fairly unaffected by HPAM concentration between 25 ppm and 2,000 ppm [in brine with 1% sodium chloride (NaCl) and 0.05% $CaCl_2$]. These findings should simplify the job of modelers when projecting the performance of polymer flooding.

Introduction

The most common polymer used in polymer flooding and enhanced oil recovery is HPAM (an abbreviation for partially hydrolyzed polyacrylamide or acrylamide-acrylate copolymer). Rheological properties of polymer solutions in porous media are often required for modelers/simulators when projecting the performance of a polymer flood. Especially for vertical polymer injection wells, an injected solution could conceivably experience a wide range of velocities as it enters the porous rock and propagates radially away from the wellbore. During polymer flooding, the velocities where shear thickening occurs directly impact HPAM injectivity, fracture initiation, and whether viscoelasticity is significant in oil recovery of capillary-trapped residual oil with or without the presence of fractures (Seright 1983; Seright et al. 2009, 2011; Seright and Wang 2023a, 2023b; Khodaverdian et al. 2010; Ma and McClure 2017; Azad and Trivedi 2020a, 2020b; Rock et al. 2020; Hwang et al. 2022; Sagyndikov et al. 2022; AlAbdullah et al. 2023; Li et al. 2023; Azad and Seright 2025).

Our goal with this paper is to provide important experimental data and trends for HPAM (18–20 million g/mol Mw, 30% degree of hydrolysis) rheology in permeable sandstone as a function of salinity, divalent calcium content, and polymer concentration. which are important to modelers and reservoir simulators when projecting the performance of polymer floods. First, we briefly review HPAM rheology reported previously in permeable porous media (e.g., >200 md sandstone)—including general shape of the rheological curves and effects of polymer concentration, rock permeability, oil saturation (S_{or}), Mw, and salinity. [Incidentally, virtually all existing medium- to large-scale polymer floods have been applied in reservoirs with average permeability greater than 200 md (Seright and Wang 2023a).] Then, after summarizing our materials and methods, we present HPAM rheology in a 738-md sandstone as a function of salinity (from 0.1% to 10% TDS) and contrast it with a similar, previous study using a 252-md sandstone. The new study includes examining HPAM rheology (in sandstone) at a fixed salinity (1% TDS) but with hardness levels ranging from 0 ppm to 1,000 ppm $CaCl_2$. In brine with 1% NaCl and 0.05% $CaCl_2$, rheology in sandstone was determined for HPAM concentrations between 25 ppm and 2,000 ppm. We also report "entrance pressure drops" and levels of mechanical degradation (alternatively called "shear" or more appropriately, "extensional" degradation or "mechanical degradation in an extensional flow field") exhibited as a function of Darcy velocity. The discussion includes the practical implications of our findings for polymer flooding, as well as their theoretical implications.

Background: HPAM Rheology in Porous Media

General Shape of Rheological Curves and Effect of Polymer Concentration. Fig. 1 shows the rheology (resistance factors) of HPAM (18–20 million g/mol Mw) in a 5,120-md core as a function of Darcy velocity and polymer concentration (from 0 ppm to 2,500 ppm). This figure illustrates many of the regimes exhibited by HPAM solutions in porous media. Resistance factor is defined as brine mobility divided by polymer solution mobility. One may think of the resistance factor as the effective viscosity of the polymer solution (relative to water) in porous media. HPAM solution viscosity and resistance factor increase with increased polymer concentration. At very low velocities (depending on rock permeability and polymer Mw and concentration), Newtonian behavior may be seen (Seright et al. 2011).

*Corresponding author; email: randy.seright@nmt.edu

This paper (SPE 224231) was accepted for presentation at the SPE International Conference on Oilfield Chemistry, Galveston, Texas, USA, 9–10 April 2025, and revised for publication. Original manuscript received for review 11 April 2025. Revised manuscript received for review 5 May 2025. Paper peer approved 6 May 2025.

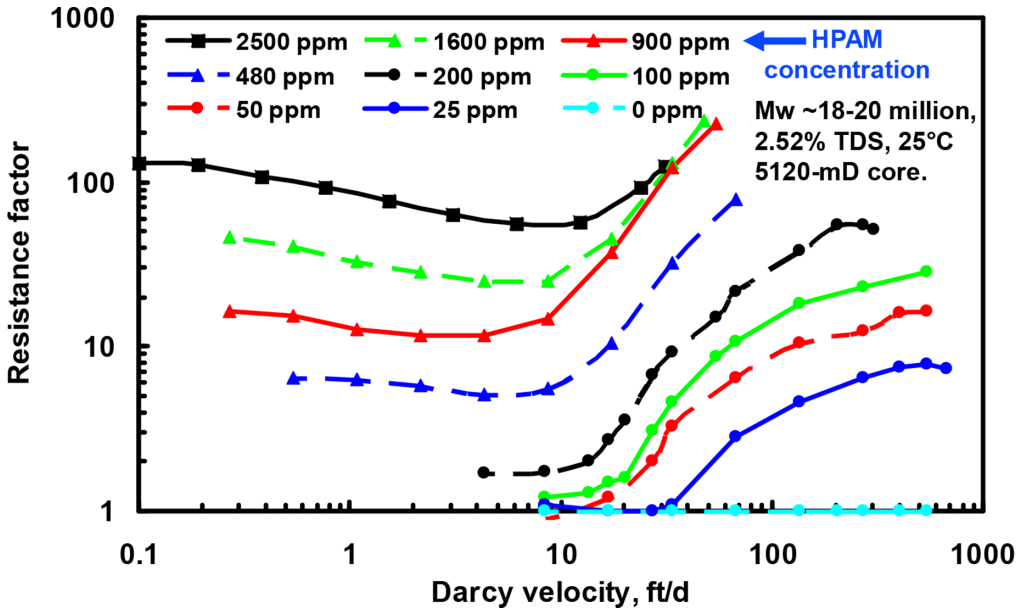

Fig. 1—Effect of velocity and HPAM concentration on rheology in a 5,120-md core (Seright et al. 2011).

If the polymer concentration is low, a Newtonian regime is expected until a relatively high velocity is reached [**Fig. 1** of this paper; Chauveteau and Moan (1981), their Fig. 4; Seright (2017), their Fig. 14].

Shear thinning may occur as the rate increases (e.g., 0.2–10 ft/D in **Fig. 1**). Resistance factor vs. velocity in porous media mimics viscosity vs. shear rate in a Couette viscometer at low-moderate shear rates (Delshad et al. 2008; Seright et al. 2011). The lower the permeability, the lower the velocity at which the onset of shear thinning occurs (Cannella et al. 1988; Seright et al. 2011). Shear thinning may not be seen if the polymer concentration is low. The two main reasons are (1) that shear thinning decreases when polymer concentration decreases (when polymer concentration tends toward zero, the shear-thinning character of any polymer solution disappears since the solution tends toward the Newtonian behavior of water) and (2) that pressure sensors used for measuring resistance factors are not sensitive enough to explore the low Darcy velocities domain (velocities lower than 10 ft/D in **Fig. 1** for the solutions in the concentration range of 25–200 ppm). In **Fig. 1**, shear thinning is only noted at and above 480 ppm HPAM, which is above the critical overlap concentration (C^*) of 200 ppm. [Using the method of Jouenne and Levache (2020), this C^* value was estimated from zero-shear-rate viscosities for this polymer in brine with 2.52% TDS.]

As the velocity is increased further (e.g., above 10 ft/D in **Fig. 1**), resistance factor increases with increased rate. In the petroleum literature, this behavior has commonly been called "shear thickening," although others have characterized it "dilatant," "pseudodilatant," "rheo thickening," "extensional thickening," "flow thickening," "porous-media thickening," "elastic turbulence," or "viscoelastic" (Chauveteau and Moan 1981; Chauveteau 1981; Durst et al. 1982; Heemskerk et al. 1984; Southwick and Manke 1988; Masuda et al. 1992; Seright et al. 2011; Howe et al. 2015; Jouenne et al. 2018; Jouenne and Heurteux 2019; Azad 2023). As shown in **Fig. 1**, shear thickening was observed for all HPAM concentrations from 25 ppm to 2,500 ppm—thus, in a concentration domain from dilute to semidilute nonentangled regimes. Indeed, the entanglement concentration, C_e, is approximately 10 C^* for neutral polymers in good solvent (Colby 2010; Jouenne and Levache 2020), which suggests that $C_e \sim 2{,}000$ ppm for this polymer/brine system. Interestingly, shear thinning is not evident in the dilute regime (HPAM concentration below C^*), but shear thickening is prominent.

At very high velocities (not shown in **Fig. 1**), HPAM solutions experience permanent loss of viscosity and resistance factor (commonly labeled "mechanical" degradation)—manifested by resistance factors irreversibly appearing to decrease with increased rate (Seright et al. 1981; Seright and Wang 2023a).

Brief Discussion of Shear Thickening of Polymer Solutions in Porous Media. The onset of shear thickening is thought to correspond to the appearance of elastic instabilities that result from the accumulation of elastic stresses that cannot relax. They may result in secondary flows, vortices, eddies, and dead zones (Chen and Datta 2024), which modify the flow field and may lead to local pressure fluctuations from instabilities with spatial and temporal fluctuations (Ekanem et al. 2022; Sasmal 2023). Determining their onset and their effect on pressure drop is a long-standing and very complex problem of understanding the interplay between solution rheology, the flow field imposed by the geometry, the evolution (time and/or history dependence) of this flow field, and the evolution of the chain and network microstructure (such as polymer rigidity, entanglements, and polydispersity) (Yin et al. 2024). Several dimensionless parameters have been proposed: The Weissenberg number, We (which compares the strength of elastic to viscous stresses and the relaxation time of the polymer solution to the characteristic time of the shear flow); the Deborah number, De (which compares the relaxation time of the polymer solution to the residence time during which the flow field is experienced), or the product of these two parameters as proposed by McKinley et al. (1996). Different relaxation times and characteristic lengths of the flowing geometries can be involved. For example, for shear-thinning solutions, the relaxation times are shear dependent (Casanellas et al. 2016). Literature on model geometries and model solutions is abundant, but there is still no unique parameter and scaling. For enhanced oil recovery polymer solutions in porous media, we face solutions with complex rheology in very complex geometries with minimum information on local phenomena. The heterogeneity and topology of the pore network are often described solely by the two macroscopic characteristics—core porosity and core permeability. Rheology of the solution, its interaction with the porous medium, and the evolution of the flow fields at the pore level are assessed through pressure drop measurement across several thousand pores (e.g., 4,000 contraction/expansion pairs for a core length of 2 cm, assuming a contraction/expansion length of 5 μm for extensional-dominated flow fields at the pore level).

We note in particular that Chauveteau (1981) and Chauveteau and Moan (1981) provided an early discussion of intramolecular coil-stretch transitions in glass physical models. Later, Southwick and Manke (1988) extended this work to glass bead packs and Bentheimer sandstone and provided an interpretation of high resistance to flow due to coil-stretch transitions of polymer chains—not intermolecular entanglements. They suggested that the substantial resistance factors observed in the shear-thickening regime were due to significant stored energy that accumulated in the low-entropy condition of highly stretched polymer chains. Although this view has not been universally accepted, the work in the present paper will provide strong evidence to support their position. Specifically, data from this paper will support the assertion that the cause of the "shear-thickening" effect in porous media is the coil-stretch transition of individual polymer coils. Entanglements are not relevant to the explanation of shear thickening for HPAM concentrations typically used during polymer flooding.

There are several ways to define the onset of shear thickening (u_{onset}) in porous media as described in Seright et al. (2023, their Fig. 3). The first method defines the onset as the departure from the shear-thinning behavior of the resistance factor curve (resistance factor vs. Darcy velocity). This methodology is limited since it is difficult to identify the real shear-thinning portion (without any viscoelastic effect) on the resistance factor curve. A second method defines the onset velocity as the intersection of two extrapolated lines from shear-thinning and shear-thickening regions, assuming a power law behavior for both. This method is also limited because it is necessary to define the power law behavior of the shear-thinning and shear-thickening portions. A third method defines the onset as the velocity at the minimum of the resistance factor curve ($u_{onset} = u_{min}$). This resistance factor minimum (RF_{min}) results from the competition between shear thinning and shear thickening.

As a fourth method, Jouenne and Heurteux (2019) focused on the velocity (u_{max}) associated with the maximum resistance factor (RF_{max}). This maximum and associated velocity are usually more definitive experimentally than the choices for the other three methods (mentioned in the preceding paragraph). This velocity may be correlated with the lower velocity associated with the onset of shear thickening.

Some additional comments on the complexity of the shear-thickening phenomenon are as follows: While the onset of shear thickening may occur at small strain, when fluid velocity is increased, a coil-stretch transition results in a dramatic increase in the extensional viscosity because of the stretching of the chains in porous media. Some new dependence of the resistance factor with velocity could appear compared with elastic turbulence scaling at small strain. At some critical velocity, the hydrodynamic force exerted on the stretched chain (which follows a Boltzmann distribution of probability for occurrence) becomes large enough to break the carbon-carbon bond of the polymer backbone—so polymer is mechanically degraded. The resistance factor is thus the interplay between elastic instabilities, extensional viscosity, shear viscosity with a polymer evolving in its state of extension, Mw, and polydispersity. Interestingly, although "elastic turbulence" suggests substantial pressure fluctuations, for all core experiments presented in this paper, no evidence of significant pressure fluctuations was observed. Specifically, at all rates in the shear-thickening regime, pressure fluctuations were less than 0.1% of a given pressure reading. One may argue that microscopic pressure fluctuations are damped to no observable effect between pressure taps. When invoking turbulence, one normally thinks first of the Reynolds number, where the onset of turbulence is suppressed by increasing solution viscosity and decreasing conduit flow diameter. In apparent contradiction to this concept, the onset of shear thickening (and therefore, "elastic turbulence") in porous media is largely unaffected by polymer solution concentration (for polymer concentrations above C^*) and viscosity **(Fig. 1)** and is accentuated by decreasing permeability and pore size **(Fig. 2)**.

Effect of Permeability. Polymer rheology in porous media has consistently been shown to correlate with the parameters $u/(k\phi)^{0.5}$ or $u(1-\phi)/(k\phi)^{0.5}$, where u is the Darcy or superficial velocity, ϕ is the porosity, and k is the permeability (Cannella et al. 1988; Seright et al. 2011). **Fig. 2** demonstrates this point for an HPAM solution in cores with permeabilities ranging from 17.5 md to 5,120 md. This shift of the rheological curves to higher velocity (as permeability increased) is consistent with lower elongational stresses occurring in larger pore throats (at a given flow rate). This observation has been of high value to modelers when considering permeability-porosity variations in a reservoir during simulations of chemical floods. Many models and simulators (Hirasaki and Pope 1974; Chauveteau and Moan 1981; Cannella et al. 1988; Willhite and Uhl 1988; Seright 1991; Masuda et al. 1992; Delshad et al. 2008; Lohne et al. 2017; Zeynalli et al. 2023) attempted to convert velocities in porous media to an effective "shear rate" that was hoped to be directly relatable to shear rate in a viscometer. Although most of those models have the $u(1-\phi)/(k\phi)^{0.5}$ or $u/(k\phi)^{0.5}$ factor in common, different multipliers for this factor [e.g., 0.98–6 from Cannella et al. 1988, their Table II] have been assumed.

Effect of Oil Saturation. Most previous studies of the effect of permeability on polymer rheology in porous media did not have oil present (e.g., **Fig. 2**). However, Cannella et al. (1988) and Seright et al. (2023) demonstrated that the $u(1-\phi)/(k\phi)^{0.5}$ correlating factor can work well for moderate to low velocities in porous media if an oil saturation (S_{or}) is present. With oil present, the permeability to water ($k\,k_{rw}$) at S_{or} is substituted for permeability (k) in the correlation, and $\phi(1-S_{or})$ is substituted for porosity (ϕ). **Fig. 3** illustrates this point for oil saturations between 0 and 0.55 and relative permeabilities to water (k_{rw}) between 1 and 0.03 for 1,000-ppm Flopaam 3630S™ (Mw ~19 million g/mol, 30% degree of hydrolysis). Note that in **Fig. 3**, this correlation breaks down at high velocities, where the maximum resistance factor in the viscoelastic (shear-thickening) regime (RF_{max}) decreases significantly with increased oil saturation. Several other authors also noted that the presence of oil resulted in lower-than-expected resistance factors in the viscoelastic regime (Gumpenberger et al. 2012; Skauge et al. 2018; Alfazazi et al. 2021).

Effect of HPAM Mw. Using data from Seright (2009), **Fig. 4** illustrates how the onset for shear thickening (defined by $u_{onset} = u_{min}$) varies with HPAM Mw. This data was collected for commercial HPAM samples with ~30% degree of hydrolysis in a 2.52% TDS brine. For each polymer Mw, rheology in porous media was determined over a wide range of velocities in 55-md Berea sandstone, 269-md Berea sandstone, and 5,120-md porous-polyethylene cores. For plots of resistance factor vs. superficial velocity (Seright 2009, their Figs. 41 through 48), data were correlated with the parameter, $(1-\phi)/(\phi k)^{0.5}$, and the velocity at which resistance factor was minimum (u_{min}) in these plots was defined as the parameter, u_{onset}, expressed in ft/(D-md)$^{0.5}$. The correlation (red curve) in **Fig. 4** indicates that for a given permeability, the onset of shear thickening varies (approximately) inversely with the square of HPAM Mw. Howe et al. (2015) and Clarke et al. (2016) also reported this behavior.

Effect of Temperature. Seright et al. (2023) also noted that velocity dependence of HPAM resistance factor curve vs. velocity curve shifted to higher velocities as temperature increased. In particular, between 20°C and 60°C, the onset velocity of shear thickening (defined as $u_{onset} = u_{min}$) shifts upward by about a factor of 1.5 for each 20°C rise in temperature, while the viscosity of water decreases by a factor

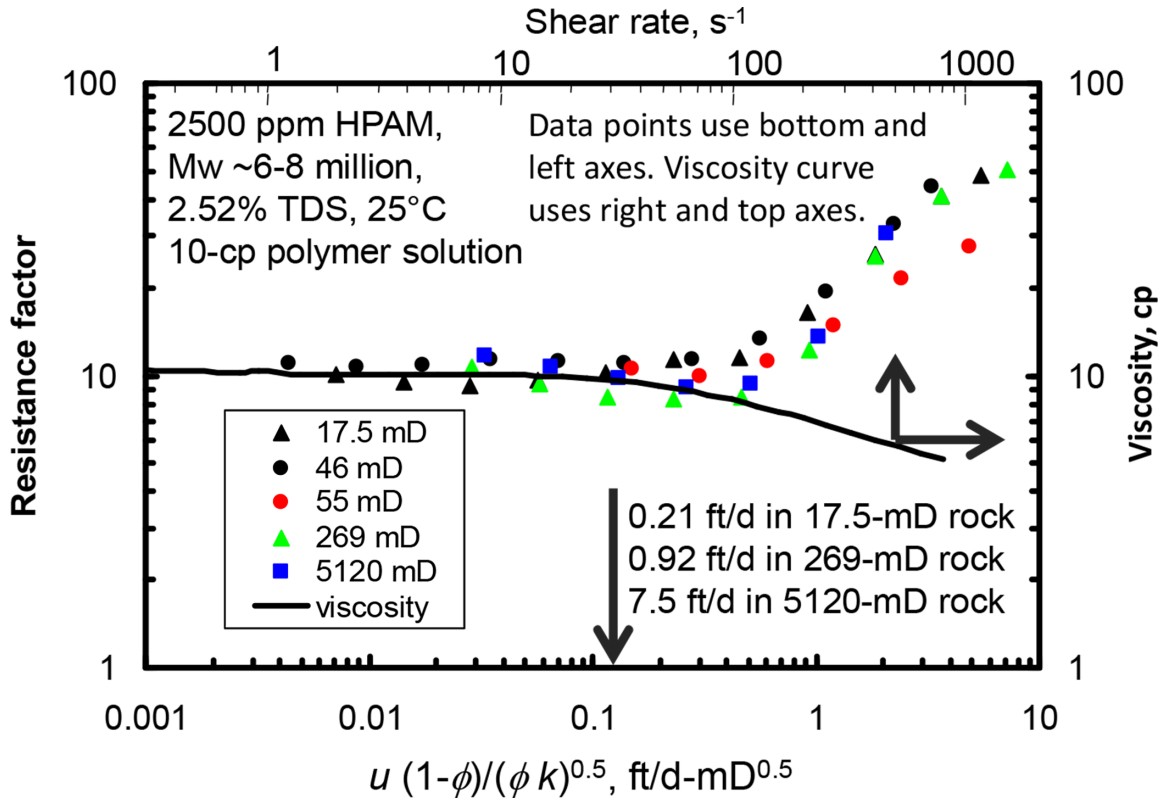

Fig. 2—Resistance factor vs. viscosity comparison (Seright et al. 2011).

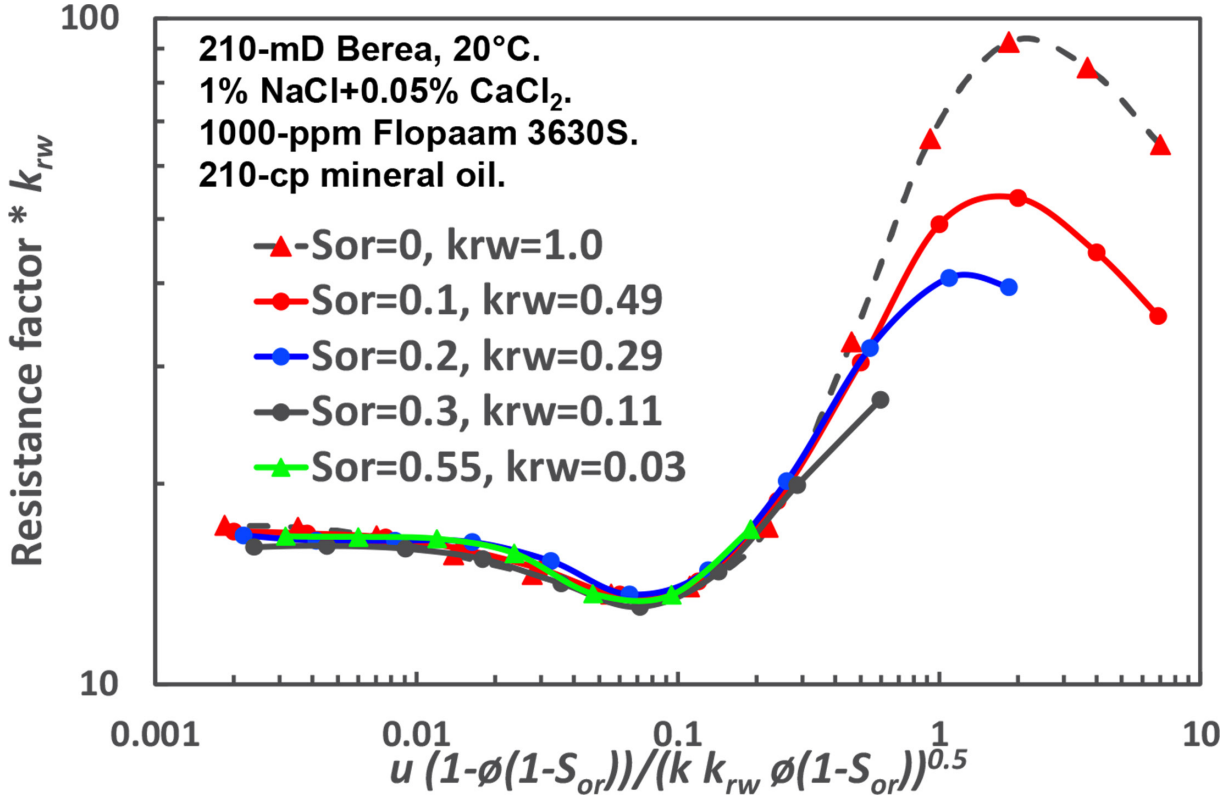

Fig. 3—Correlating rheology incorporating S_{or} into aqueous-phase porosity (Seright et al. 2023).

of about 1.5 for each 20°C rise in temperature. Nguyen and Kausch (1990) studied the dependence of degradation with solvent viscosity under steady-state and transient elongational flow—concluding that a velocity dependence with the inverse of solvent viscosity indicates that chains obey a free-draining model in which the molecular stress at the origin of chain deformation is solely determined by the friction

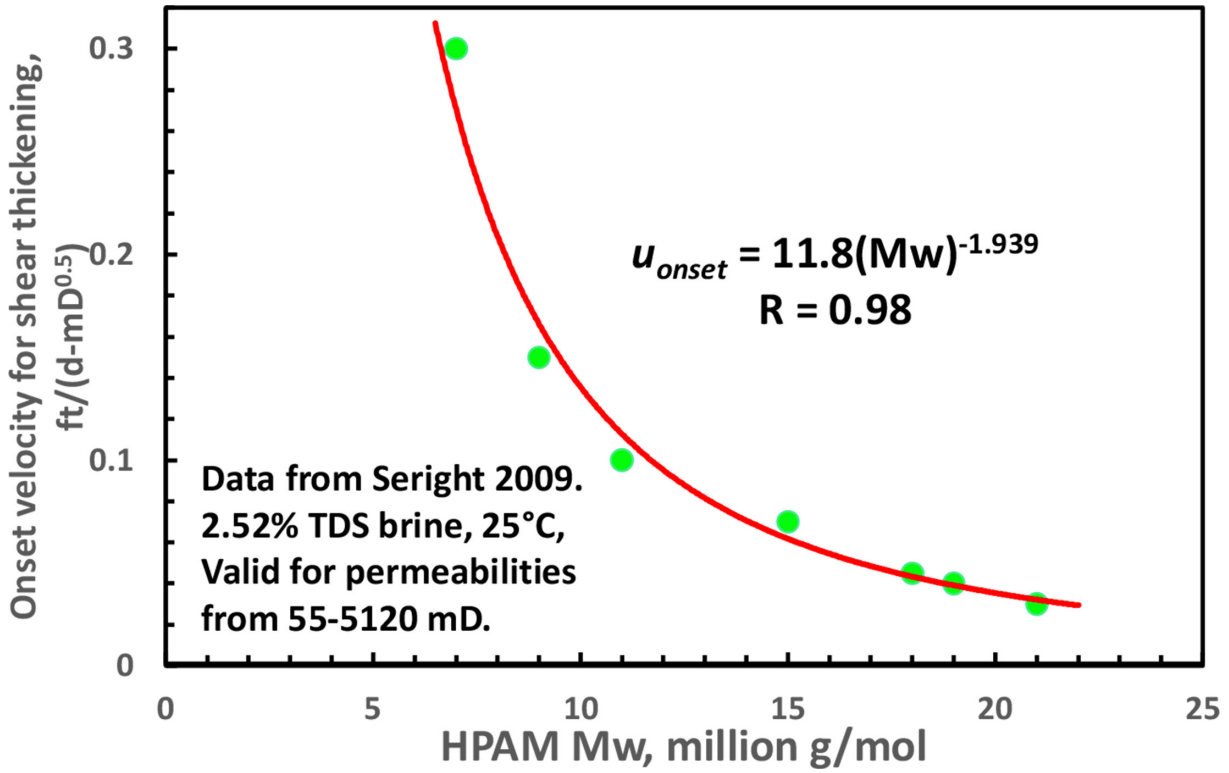

Fig. 4—Effect of HPAM Mw on onset velocity for shear thickening in porous media.

action of the solvent. In other words, the observed temperature dependence is consistent with the expected increased Rouse-Zimm relaxation times of polymer coils at higher temperatures.

Effect of Salinity. From the injection of 1,000-ppm HPAM solutions into a 204-md core, Seright et al. (2023) noted that the velocity dependence of HPAM resistance factor curve vs. velocity curve did not shift much over a wide range of salinity (i.e., from 0.105% to 5.25% TDS). This trend was confirmed for 2,000-ppm HPAM solutions with the same salt compositions injected into a 252-md core, as shown in **Fig. 5**. Of course, the magnitude of viscosity and resistance factor can increase substantially with decreased salinity, especially for salinities below 1% TDS. For both 1,000-ppm and 2,000-ppm Flopaam 3630S HPAM in ~200 md Berea sandstone, whatever the salinity in the range 0.105–5.25% TDS, the minimum resistance factor (RF_{min}) occurred at u_{min} ~ 0.5 to 1 ft/D Darcy velocity, and the maximum in the shear-thickening regime (RF_{max}) occurred at u_{max} ~ 8 ft/D. At 10.5% TDS salinity, the onset velocity for shear thickening shifted to somewhat higher velocity, but the shift was marginal. One might interpret this finding as the conformational rotation transitions of the polymer segments have about the same energy transition barriers, regardless of the initial conformation. (The purple curve with the "x"s in **Fig. 5** and subsequent figures shows onset velocities predicted from a model that will be described in the "Discussion" section.)

Doubt was expressed by Dwarakanath et al.[i] for the data shown in **Fig. 5**, claiming that Flopaam 3630S HPAM would not adequately penetrate or propagate through ~200-md rock and suggesting (without evidence) that the results may not be applicable to rocks with other permeabilities. Interestingly, we have injected Flopaam 3630S into 100–300-md Berea sandstone during many corefloods over 20 years and have never seen any problem with face plugging, high polymer retention, or polymer propagation. Furthermore, in the experiments in question associated with **Fig. 5**, more than 200 pore volumes of polymer were injected, with no sign of (1) face plugging, (2) resistance factors (in either section of the core) increasing over time, or (3) low-velocity resistance factors being substantially greater than measured viscosities.

Dwarakanath et al. suggested that our findings (shown in **Fig. 5**) were inconsistent with previous literature, although no elaboration or evidence was provided. In our examination of the literature, we note that Heemskerk et al. (1984) speculated that the velocity for the onset of shear thickening should increase with increased salinity. However, Heemskerk et al. provided no evidence to support their claim.

While examining the data of Yuan (1981), Delshad et al. (2008) also suggested that the velocity for the onset of shear thickening in porous media increases with increasing salinity. However, this suggestion was based on attempts to match viscosity vs. shear rate curves (from a viscometer) with resistance factor vs. velocity curves (from corefloods). As revealed by Seright et al. (2023), this sort of matching can be quite arbitrary and lead to substantial uncertainty in the velocity chosen as the onset for shear thickening. In re-examining Yuan's data (Delshad et al. 2008, their Figs. 5 and 6), we note that Yuan's minimum resistance factor for 1,000-ppm Pusher 700 HPAM in 1% NaCl occurred at the same velocity as in 0.1% NaCl. Furthermore, Yuan's maximum resistance factor in the shear-thickening regime in 1% NaCl occurred at the same velocity as in 0.1% NaCl. These observations are consistent with **Fig. 5** and other findings by Seright et al. (2023).

[i]Dwarakanath, V. et al. . et al. 2023. Personal communication concerning SPE paper SPE-215060-MS.

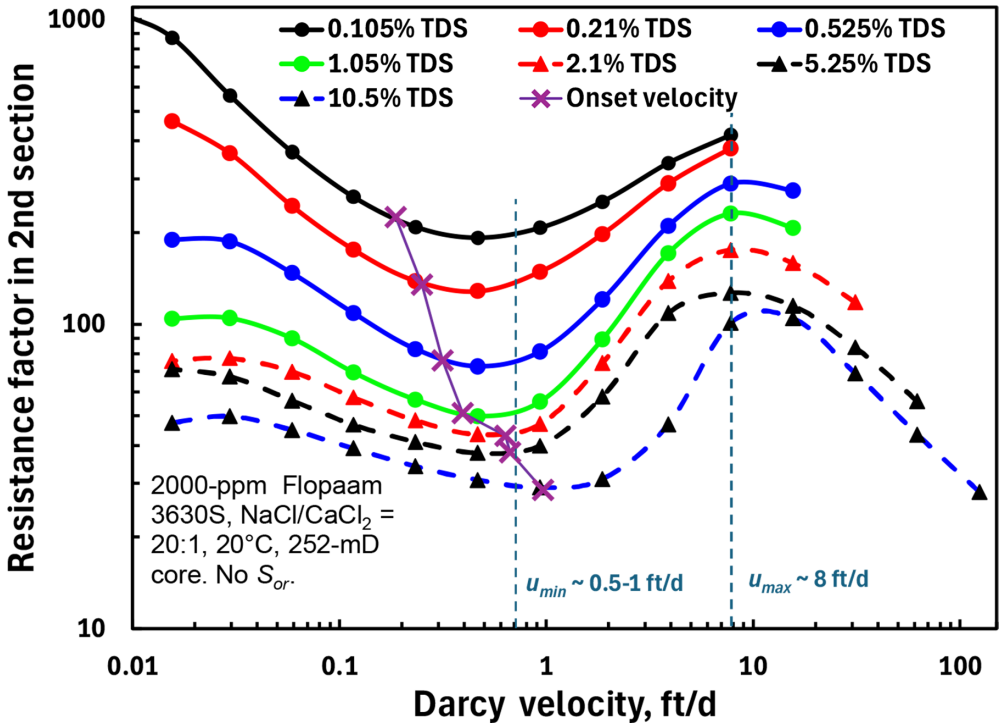

Fig. 5—Resistance factor vs. rate and salinity in the 252-md Berea sandstone (Seright et al. 2023).

A notable number of studies of synthetic polymer rheology in porous media have been conducted using a wide range of conditions (e.g., Jennings et al. 1971; Hirasaki and Pope 1974; Seright 1983; Masuda et al. 1992; Seright et al. 2009, 2011; Howe et al. 2015; Lohne et al. 2017; Seright 2017; Masalmeh et al. 2019; Wang et al. 2020; Seright et al. 2021; Alfazazi et al. 2021; Sagyndikov et al. 2022; Zeynalli et al. 2023). Delshad et al. (2008), Lohne et al. (2017), Azad and Trivedi (2019), Jouenne and Heurteux (2019), and Zeynalli et al. (2023) formulated models/equations that were used to characterize many published data sets for rheology in porous media. However, the diverse combination of polymer Mw, concentration, source, salinity, temperature, and core material does not allow definitive conclusions to be made on the effects of salinity on the velocity dependence of HPAM rheology in porous media, especially the velocity for the onset of shear thickening.

In a short (2.54-cm-long), 9-darcy ceramic core, Jouenne and Heurteux (2019) studied Flopaam 3630S HPAM solutions with different salinities. In agreement with **Fig. 5** (where permeability was 252 md), Fig. 9 of Jouenne and Heurteux shows that the rates associated with the minimum and maximum resistance factors were weakly dependent on salinity and hardness between 0.04% TDS and 5.6% TDS (with 800 ppm HPAM in a 9-darcy core).

In a viscometer, while testing polyacrylamide/water glycerol solutions, Briscoe et al. (1999) noted that increasing the salinity from 2% to 5.85% NaCl had no discernable effect on the shear rate for the onset of shear thickening. Azad (2023) reported that varying the salinity from 0.5% to 2% did not affect the onset of shear thickening for 0.1% Flopaam 3630S HPAM.

Zaitoun et al. (2012) argued that the tighter coils at higher salinities cause HPAM molecules to be less prone to disentangle and elongate when forced through pore throats at higher rates—thus making them more susceptible to mechanical degradation as salinity increases.

In summary, although there is a common misconception that the onset of shear thickening will shift to significantly higher velocities as salinity increases [perhaps, because of the early, unsupported suggestion by Heemskerk et al. 1984], the available data in the literature does not support this claim. Consequently, the goal of this work is to clarify the effect of salinity on the onset velocity, especially in a more permeable core and using a wide range of salinity and divalent ion content for HPAM solutions.

Materials and Methods

Polymer and Solutions. The HPAM polymer used in this work was SNF Flopaam 3630S, lot #GJ1201. The manufacturer indicated that this copolymer contained ~70% acrylamide groups and ~30% acrylate groups, with a Mw of 18–20 million g/mol. Polymer solutions were prepared by sprinkling HPAM onto the shoulder of a vortex created using IKA20 overhead stirrers (at 300 rev/min using 3-in.-long, four-paddle blades). Solutions were stirred overnight.

Polymer solution viscosities were measured using a Vilastic V-E rheometer. Viscosity vs. shear rate data for the solutions used in this work are characterized in Appendix A of Seright et al. (2025). From each polymer solution, intrinsic viscosity [μ] was estimated with the model of Jouenne and Levache (2020). For brines with NaCl/$CaCl_2$ = 20:1, the zero-shear viscosity was 10–14 times greater at 0.105% TDS than at 10.5% TDS, depending on polymer concentration. Also, with 0.105% TDS, zero-shear viscosity was 4.5 times greater with 2,000 ppm HPAM than with 1,000 ppm. With 10.5% TDS, zero-shear viscosity was 3.3 times greater with 2,000 ppm HPAM than with 1,000 ppm HPAM.

As expected, viscosity decreased with increasing salinity. For 2,000 ppm HPAM in brines with salinity less than 2% TDS, **Fig. 6**(left) shows that the zero-shear viscosity decreased with increased salinity, raised to the power −0.707 (i.e., $-1/\sqrt{2}$). In this figure, the green squares were taken from Seright et al. (2025, their Fig. A-2), which represents the first set of viscosities with solutions containing 20:1 NaCl/$CaCl_2$. The blue circles were taken from Seright et al. (2025, their Fig. A-3), which represents the second set of viscosities with solutions containing 20:1 NaCl/$CaCl_2$. The red triangles were taken from Seright et al. (2025, their Fig. A-4), which contained NaCl with no $CaCl_2$. When the same figure is plotted with intrinsic viscosity,

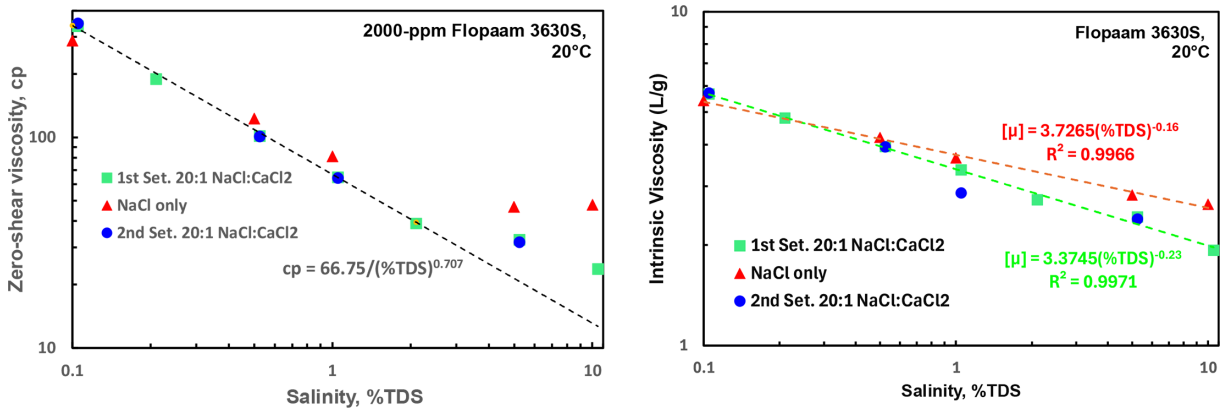

Fig. 6—Effect of salinity and calcium on (left) zero-shear viscosity and (right) intrinsic viscosity. For polymer below 2% TDS, zero-shear-rate viscosity varies with salinity raised to the power –1/√2. Over the entire salinity range, intrinsic viscosity obeys the power law dependence with an exponent of –0.16 for NaCl only and –0.23 for 20:1 NaCl/$CaCl_2$ brines.

$[\mu]$, instead of zero-shear viscosity (**Fig. 6**, right), a power law dependence of the salinity ($[\mu] \propto (\%\text{TDS})^{Sp}$) is obtained with an exponent Sp of −0.16 for polymer solutions in NaCl only and −0.23 in 20:1 NaCl/$CaCl_2$ solutions.

In brines containing 1% TDS, the zero-shear viscosity decreased only 6% (from 82.3 cp to 77.4 cp) as the $CaCl_2$ content increased from 0 ppm to 200 ppm. However, as $CaCl_2$ content was further raised to 476 ppm and 1,000 ppm, the zero-shear viscosity decreased to 61.8 cp and 46.8 cp, respectively (25% and 44% reductions, respectively), compared with the case with NaCl only. Thus, as expected, calcium cations have a greater effect on HPAM viscosity than sodium cations. At fixed anionicity, the zero-shear viscosity depends on the balance between divalent and monovalent chain dynamics (because of charge screening and labile structuring).

Cores and Corefloods. Berea or Dundee sandstone cores were used in this work, with porosity of 0.21 and absolute permeability (to water) ranging from 252 md to 838 md. [The 252-md core was used by Seright et al. (2023), while the 738- and 838-md cores were used in the present work.] The cores were 2.54 cm in diameter and 15.24 cm in length, with an internal pressure tap located 7.62 cm from the inlet core face. Dry cores were placed within a CoreLab rubber sleeve and confined with 1,500 psi pressure. After core evacuation and saturation with brine, permeability was quite constant through the different sections of the cores. For a given set of experiments, the experiment with the highest salinity was done first, followed by progressively less-saline solutions. At a given salinity, the highest rates

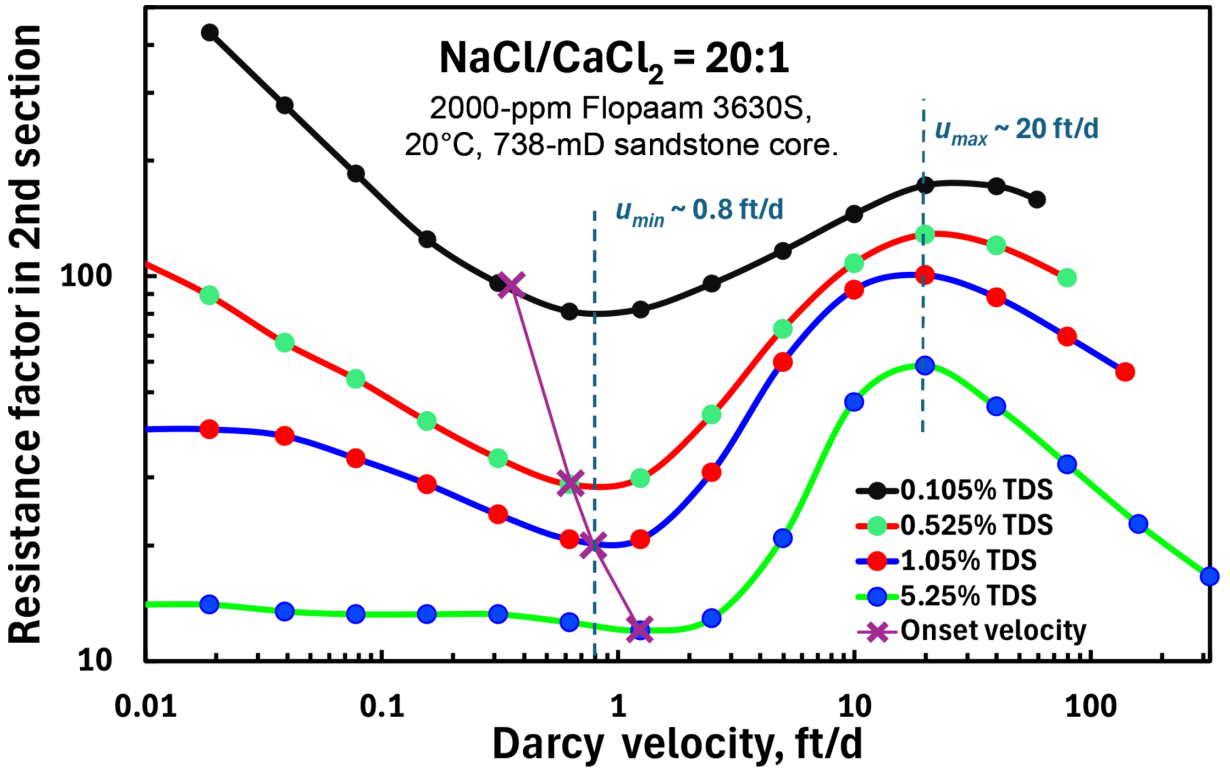

Fig. 7—Resistance factor vs. rate and salinity in the 738-md Berea sandstone.

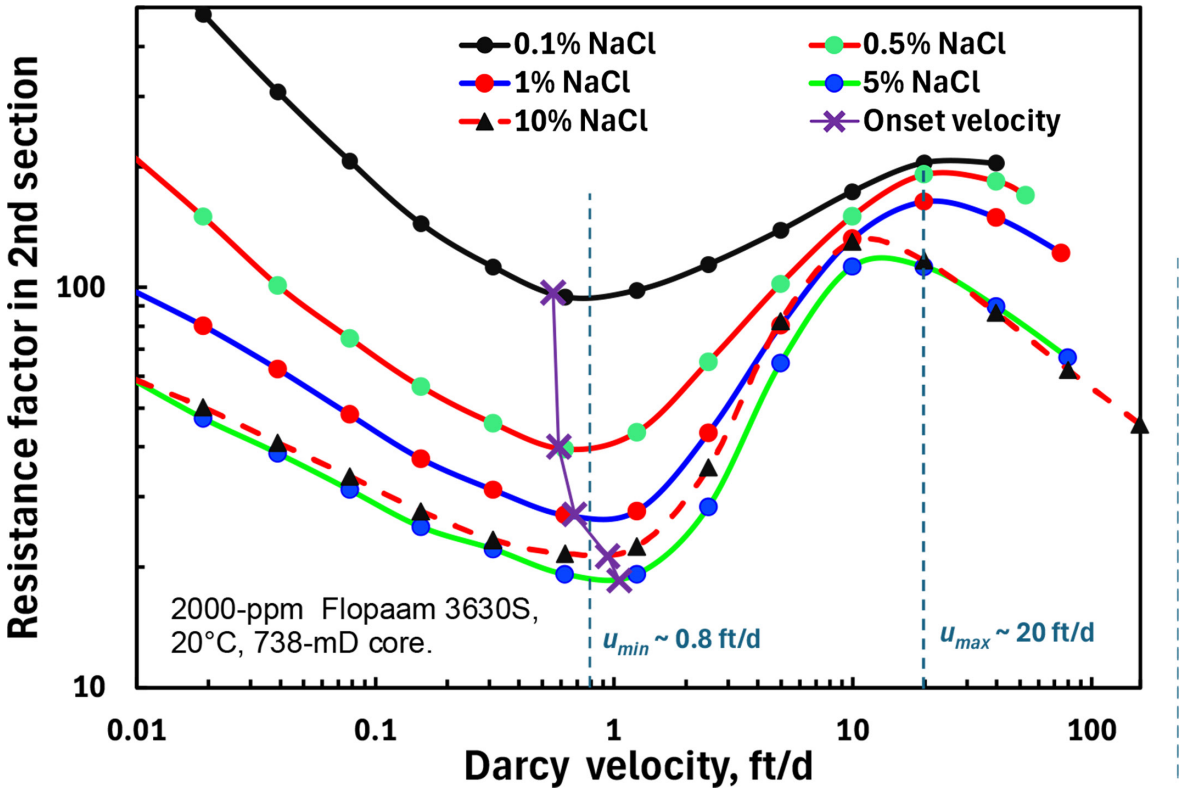

Fig. 8—Resistance factor vs. rate and NaCl content in the 738-md Berea sandstone.

were applied first, followed by progressively lower rates. Several pore volumes of fluid were flushed for stabilization for each case (except at the lowest rates).

Results

Effect of Permeability on Rheological Shift. Because of the skepticism expressed about the results in **Fig. 5** (Dwarakanath et al.), we repeated experiments using a more permeable (738-md Berea sandstone) core. The results are shown in **Fig. 7** for salinities of 0.105%, 0.525%, 1.05%, and 5.25% TDS with $NaCl/CaCl_2$ = 20:1. The minimum in the resistance factor curves (RF_{min}) occurred at a Darcy velocity (u_{min}) of about 0.8 ft/D, while the maximum resistance factor (RF_{max}) in the high-velocity shear-thickening region occurred at a u_{max} of about 20 ft/D. These values compare with about 0.5 ft/D and 8 ft/D in the 252-md Berea sandstone **(Fig. 5)**. This shift of the rheological curves to higher velocities (as permeability increased) is quantitatively consistent with the capillary-bundle shift factor, $(1 - \phi)/(k\phi)^{0.5}$ (Seright et al. 2011). Especially, note that for a given rock permeability, the velocities at which the onset of shear thickening occurred (when defined as $u_{onset} = u_{min}$) were very weakly dependent on salinity over a wide range (**Figs. 5 and 7**). The shear-thickening onset (u_{min}) shifted to slightly higher velocities at the highest salinity. Further work is needed to explain why the positions of the u_{min} and u_{max} values are at the highest salinity. We speculate that the behavior may be related to the deterioration of solvent quality (and HPAM solubility) at the highest salinity.

Rheological Shift in NaCl Brines. Since the experiments shown in **Figs. 5 and 7** were conducted with an $NaCl/CaCl_2$ ratio of 20:1, the experiments in **Fig. 7** were repeated in brines that contained only NaCl (i.e., no $CaCl_2$). **Fig. 8** demonstrates that the resistance factor curves show the same velocity locations for the minima and maxima for the NaCl brines as for the brines with a fixed $NaCl/CaCl_2$ ratio of 20:1. Again, the velocities at which the minima and maxima occur (u_{min} and u_{max}) were not strongly dependent on salinity over a wide range.

Effect of $CaCl_2$ Content with 1% TDS. To further explore the effect of calcium, experiments were performed with a fixed total salinity of 1% TDS, but with varying content of $CaCl_2$ (the remainder of the salinity consisted of NaCl). For $CaCl_2$ contents ranging from 0 ppm to 1,000 ppm, **Fig. 9** demonstrates that the resistance factor curves in NaCl show velocity locations for the minima and maxima for the NaCl brines similar to those for the brines with a fixed $NaCl/CaCl_2$ ratio of 20:1. The velocities at which the minima and maxima occur were fairly invariant to $CaCl_2$ content over a wide range. The onset velocity (u_{min}) shifted to slightly higher values at the highest $CaCl_2$ concentrations—perhaps because of deterioration of solvent quality and solubility limitations of the HPAM.

Based on **Figs. 5 and 7 through 9, Fig. 10** plots the ratio RF_{max}/RF_{min} of maximum resistance factor (in the shear-thickening region) to minimum resistance factor for a given curve. At 0.1% TDS salinity, this ratio was about two for the cases in **Figs. 5 through 9**. This ratio increased with increased salinity up to 1% TDS. For higher salinities, the ratio of maximum to minimum resistance factor was fairly constant, for a given set of data. However, this ratio was greatest (~6) for the case with no calcium present (blue curve in **Fig. 10**). This ratio was about 4.9 for the case with $NaCl/CaCl_2$ = 20 in the 738-md Berea sandstone (red curve in **Fig. 10**). **Table A-1** in Appendix A lists velocities and resistance factor values associated with the maxima and minima.

The pressure drop measured across a core includes the contribution of the shear viscosity and that of elastic effects (including elastic instabilities and extensional viscosity). (As will be seen in the next subsection, an "entrance pressure drop" may also be seen, which is

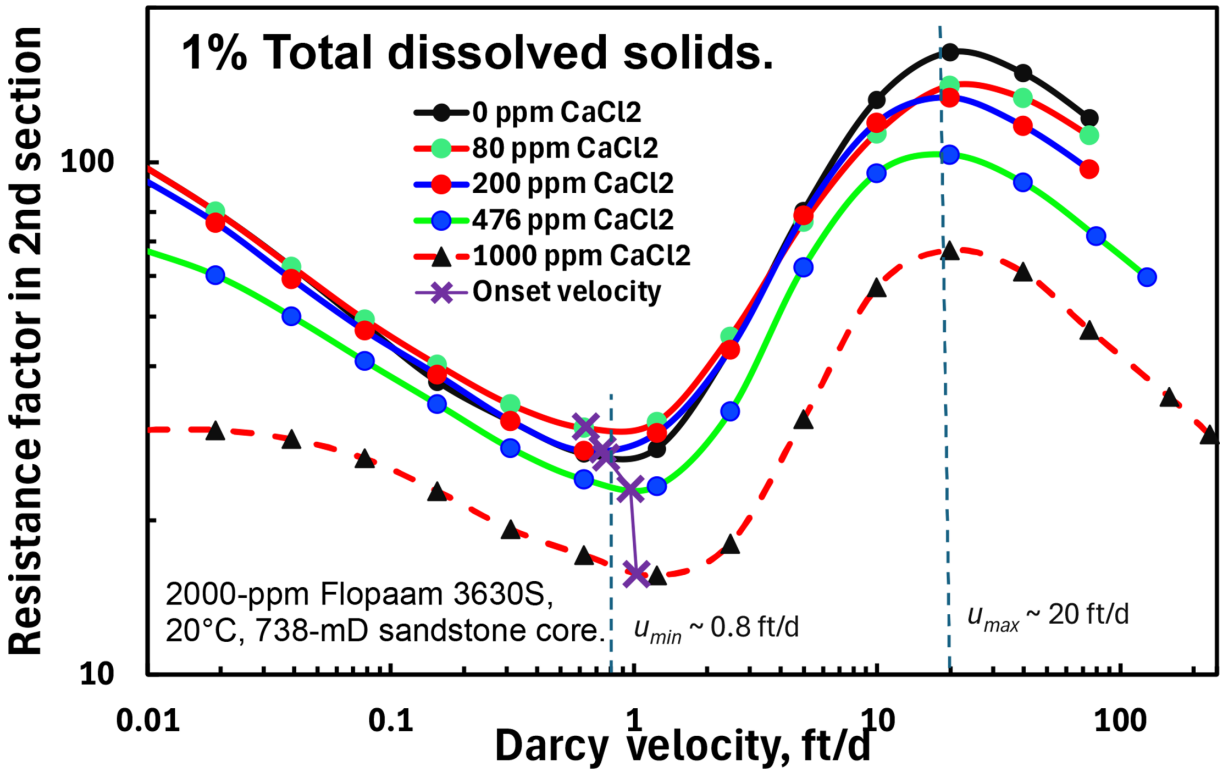

Fig. 9—Resistance factor vs. rate and $CaCl_2$ content with total salinity fixed at 1% TDS in the 738-md Berea sandstone.

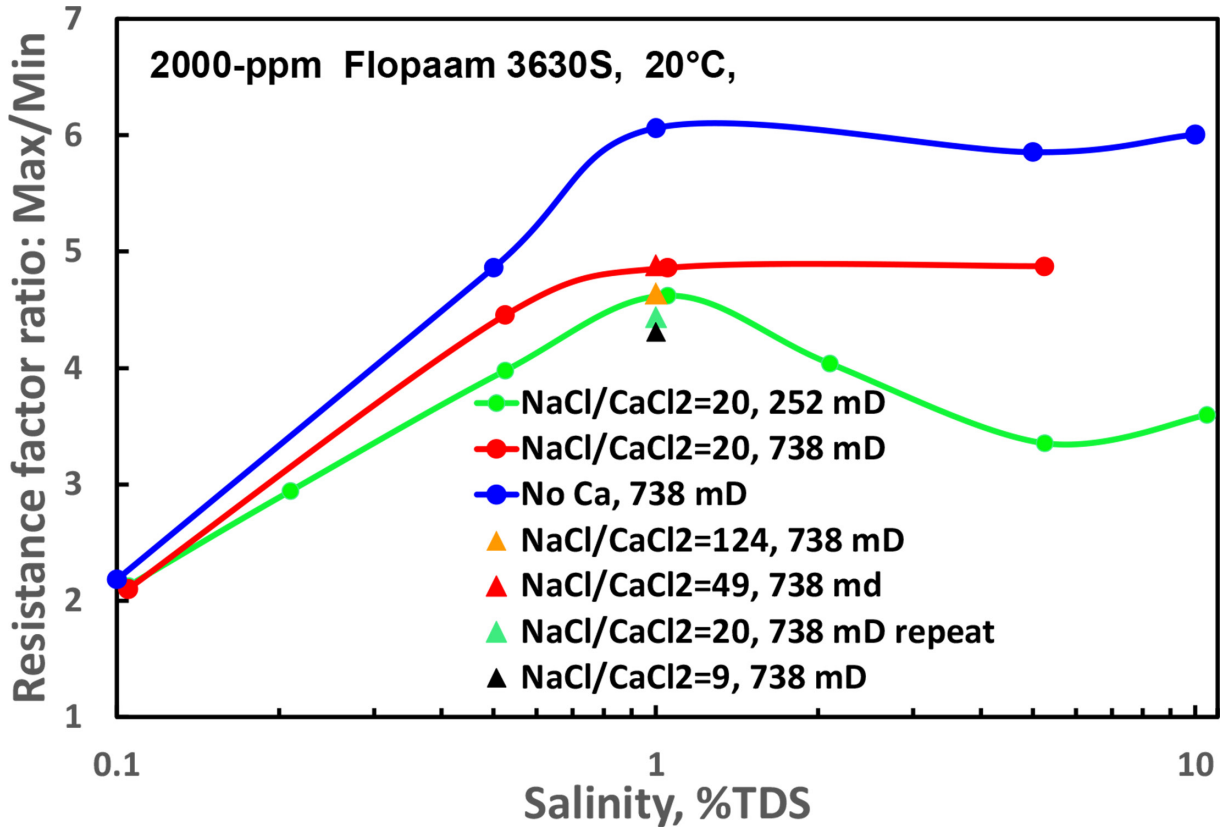

Fig. 10—Ratio of maximum to minimum resistance factors, RF_{max}/RF_{min}.

associated with mechanical degradation of the polymer.) **Figs. 7 through 9** indicate that the resistance factor is greatly affected by salinity in the low-velocity region (before the onset of shear thickening), whereas RF_{max} can be much less affected. This behavior can be explained

as follows: RF_{min} results from the contribution of shear viscosity near the onset of shear thickening, while RF_{max} results from a balance between the state where polymer chains are highly stretched and mechanical degradation of the polymer. While original chain conformation at rest (along with that under shear flow) is highly dependent on salinity, once elongated, polymer chains forget their initial conformation state—which would explain the modest dependence of RF_{max} on salinity. In other words, when polymer chains are fully stretched, the conformations are all the same, regardless of their initial condition. Thus, when salinity is increased, RF_{min} decreases substantially, while RF_{max} decreases more modestly. This also explains why the ratio RF_{max}/RF_{min} increases with salinity. Consistent with the findings in **Figs. 9 and 10**, Jouenne and Heurteux (2019) observed only a slight decrease of RF_{max} when calcium was added to a pure NaCl brine at 6 g/L. The lower viscosity of the quiescent HPAM solutions at the highest salinities may also contribute to the fact that the largest RF_{max}/RF_{min} ratios occur at the highest salinities.

Entrance Pressure Drop. Seright (1983) and Seright et al. (2009, 2023) noted that HPAM solutions can show an entrance pressure drop associated with polymer reconfiguration or mechanical degradation at high velocities. Basically, when HPAM enters a porous medium at a high velocity, a pressure drop is seen at the entrance sandface that is notably greater than expected, given the resistance factors and pressure gradients found in the remainder of the core or porous medium. Seright (1983) proposed assigning an entrance pressure drop to account for this behavior and correlated the magnitude of the entrance pressure drop with the extent of mechanical degradation exhibited by the polymer. Seright (1983) demonstrated that this entrance pressure drop was not due to filtration of polymer or gel or a progressive plugging effect. The entrance pressure drop disappears if the mechanically degraded HPAM solution from injection at a given high velocity is reinjected into the same core at the same or lower velocity (Seright 1983; Seright et al. 2009).

Figs. C1 through C4 in Appendix C of Seright et al. (2025) show the entrance pressure drops calculated for our experiments associated with **Figs. 5 through 9**. Note that the entrance pressure drop was zero below 3 ft/D and increased with increased rate. The behavior was not strongly dependent on salinity or calcium content.

Mechanical Degradation. Figs. 11 and 12 show that for a given velocity, mechanical (or shear) degradation (as measured at 7.3 s^{-1} shear rate, 20°C) became more severe as salinity/hardness increased. The *y*-axes in **Figs. 11 and 12** show the remaining viscosity expressed as $100 \times [(\mu - \mu_s)/(\mu_o - \mu_s)]$, where μ_o is the original viscosity measured at 7.3 s^{-1}, and μ_s is the solvent viscosity (i.e., 1 cp). For a given velocity and salinity, mechanical degradation becomes more severe as salinity and hardness increase, especially above 1% TDS. This observation is consistent with previous literature (Maerker 1975).

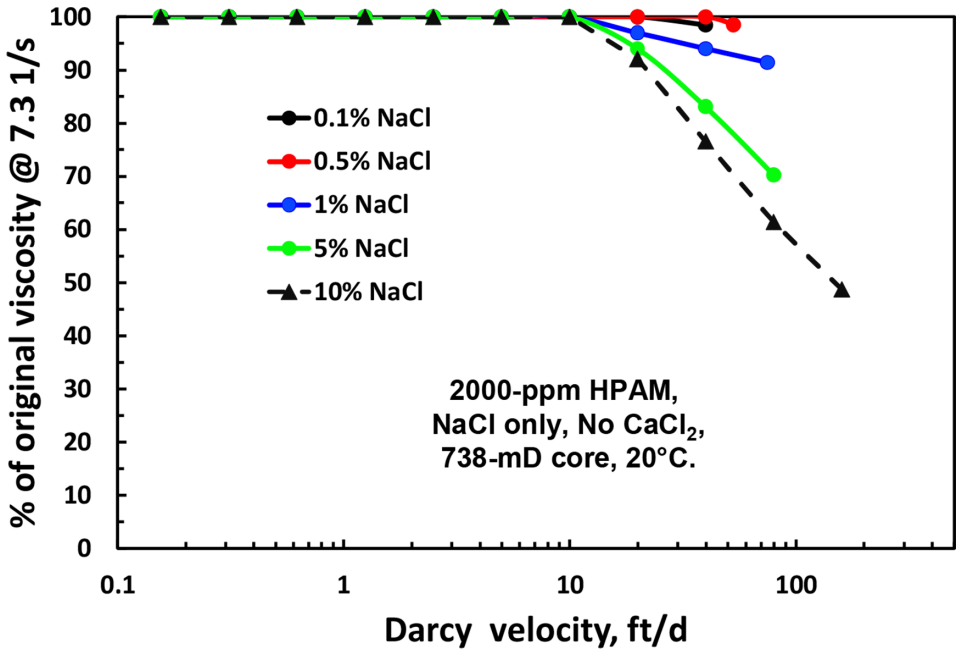

Fig. 11—HPAM mechanical degradation vs. rate and NaCl content in the 738-md Berea.

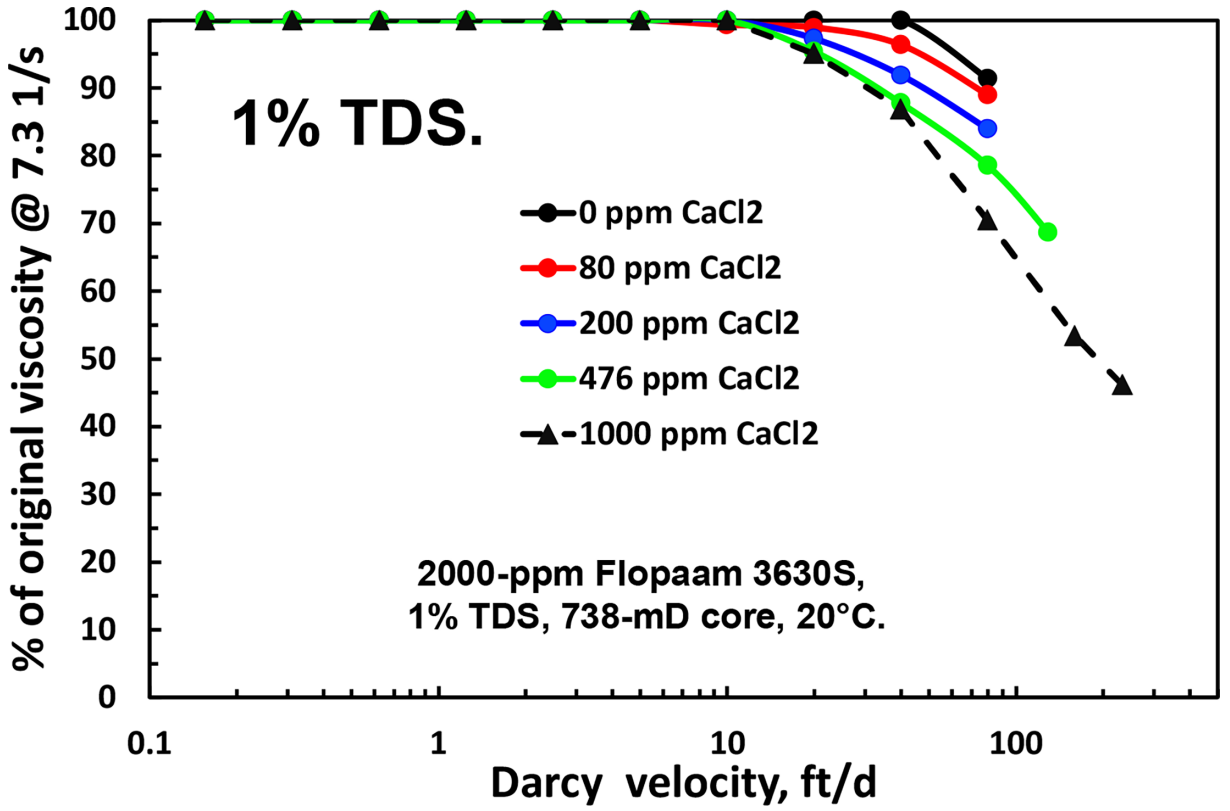

Fig. 12—HPAM mechanical degradation vs. rate and $CaCl_2$ content in the 738-md Berea.

Effect of Polymer Concentration. The effect of HPAM (Flopaam 3630S) concentration on rheology in porous media was investigated at a fixed salinity of 1% NaCl, 0.05% $CaCl_2$ at 20°C. In this work, we used a 15.24-cm-long 838-md Dundee sandstone core, with an internal pressure tap located halfway through the core. Before injecting polymer, the permeability of the core was tested over a wide range of flow rates, up to 2,486 ft/D. Permeabilities were constant up to 1,243 ft/D, with no sign of inertial effects (blue squares in **Fig. 13**). At 2,486 ft/D, an 11% increase in resistance to flow (i.e., temporary permeability reduction) indicated the onset of inertial effects (e.g., turbulence). Consequently, all experiments in this section were conducted at 1,243 ft/D or less. These experiments were conducted using the lowest polymer concentration first (i.e., 25 ppm). As with previous experiments, the highest flow rates were applied first, followed by successively lower rates, down to the lowest rate. The core confining pressure was 1,500 psi, so the highest applied rate was not allowed to generate a pressure drop any greater than 1,350 psi—which limited the maximum injection rate for the 500-ppm, 1,000-ppm, and 2,000-ppm HPAM solutions. After a given sequence of rates was applied with the 25-ppm HPAM solution, the sequence was repeated with the next higher polymer concentration (for HPAM concentrations up to 2,000 ppm, as indicated in **Fig. 13**). These procedures allowed favorable mobility ratios to exist during all displacements.

Consistent with **Fig. 1, Fig. 13** demonstrates that HPAM concentration did not strongly influence the range of velocities at which shear-thickening behavior occurs. From 250 ppm to 2,000 ppm HPAM, the maximum resistance factor occurred at the same velocity (~20 ft/D). The greatest shift in velocity for the maximum resistance factor occurred below C^*, which was about 200 ppm at this salinity. As HPAM concentration decreased from 250 ppm to 25 ppm, the velocity for the maximum resistance factor increased from ~20 ft/D to 78 ft/D. For each polymer concentration in **Fig. 13**, the last part of **Table A-1** (in Appendix A) lists maximum (RF_{max}) and minimum (RF_{min}) resistance factors observed, along with the velocities at which these maxima and minima occurred (u_{max} and u_{min}). **Table A-1** reveals that the ratio of maximum to minimum resistance factor increased from 25 ppm to 250 ppm HPAM but then decreased from 250 ppm to 2,000 ppm HPAM. Consequently, the greatest relative difference between the maximum and minimum resistance factors occurred near C^*. Because HPAM coils become greatly elongated (perhaps even completely stretched out) during elongational flow, we recognize that the true polymer critical overlap concentration under extensional flow in a porous medium may be much lower than the C^* measured using a conventional method (Jouenne et al. 2018; Garrepally et al. 2020, 2023). Here, we simply mention the conventionally measured C^* based on low-shear Newtonian plateau viscosity as a point of reference for our observations.

Note that shear thickening was prominent at polymer concentrations down to 25 ppm (one-eighth the value of C^*). This observation (along with the insensitivity of shear-thickening velocities to polymer concentration) suggests that polymer entanglements are not required or necessarily responsible for shear-thickening behavior. Consistent with the suggestions of Chauveteau (1981) and Southwick and Manke (1988), the data from this paper support the assertion that the cause of the "shear-thickening" effect in porous media is the coil-stretch transition of individual polymer coils. Entanglements are not relevant to the explanation of shear thickening for HPAM concentrations typically used during polymer flooding.

In agreement with **Figs. 1 and 13** (where permeability was either 5,120 md or 838 md, respectively), Fig. 5 of Jouenne and Heurteux (2019) shows that the rates associated with the minimum and maximum resistance factors varied weakly on polymer concentration, except for concentrations below 500 ppm HPAM (in a 9-darcy core).

Fig. 14 plots entrance pressure drops vs. Darcy velocity for the various polymer concentrations. This figure reveals that the entrance pressure drop increased notably with increased polymer concentration and velocity but was not prominent until the velocity exceeded 3 ft/D for these circumstances.

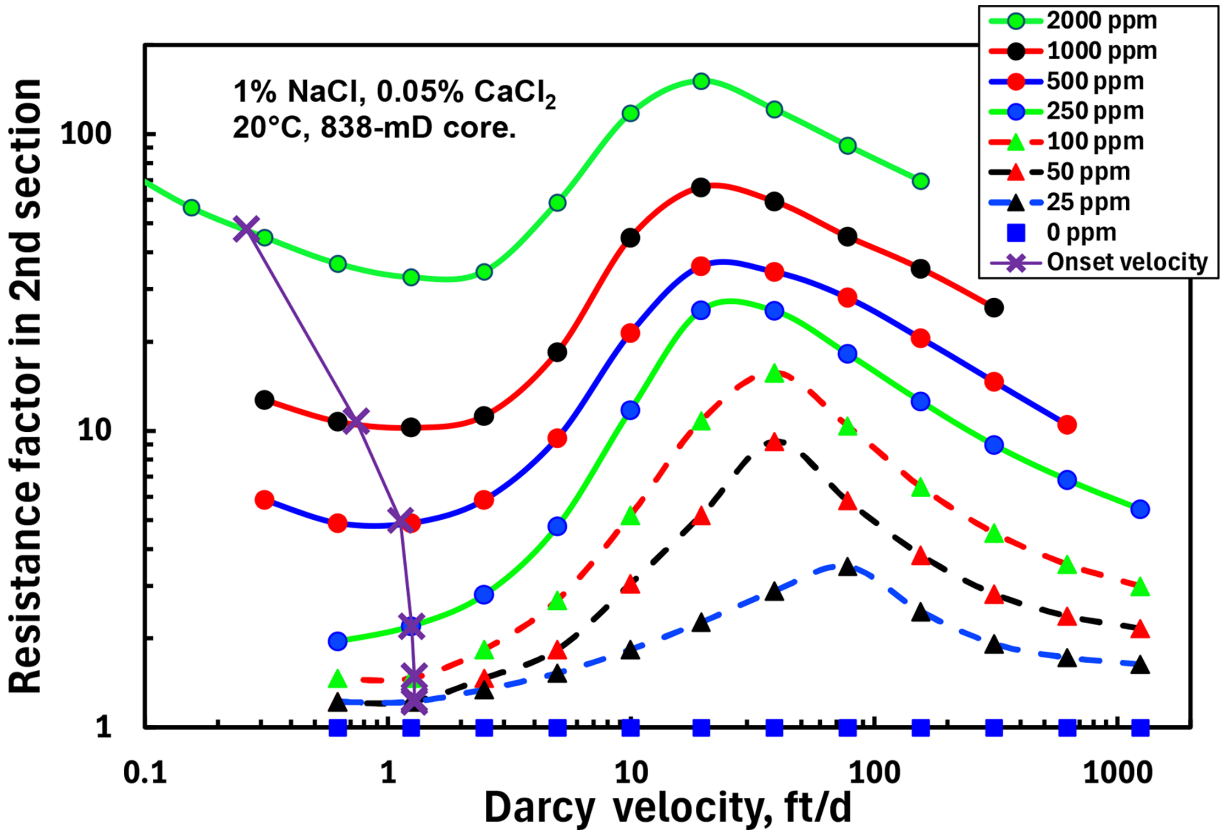

Fig. 13—Resistance factor vs. rate and HPAM concentration. Total salinity fixed at 1.05% TDS in the 838-md Dundee sandstone.

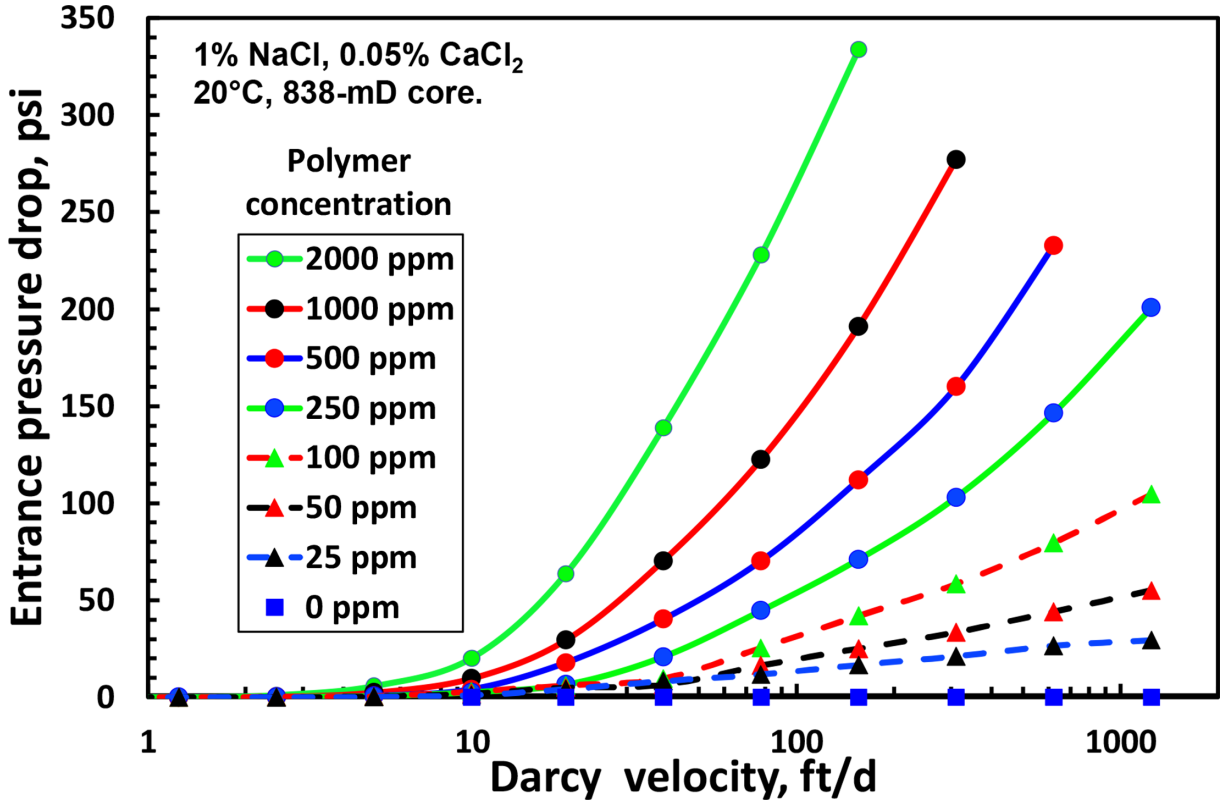

Fig. 14—Entrance pressure drop vs. rate and HPAM concentration.

During this set of experiments, effluent samples were collected, and viscosities were measured for each flow rate. The onset of degradation (i.e., viscosity loss) occurred at about the same velocity (~20 ft/D) for all polymer concentrations (Seright et al. 2025).

From these data, the remaining viscosity expressed as $100 \times [(\mu - \mu_s)/(\mu_o - \mu_s)]$, where μ is the viscosity measured at 7.3 s^{-1}, is plotted in **Fig. 15**(left). Mechanical degradation calculated from viscosity measurement at 7.3 s^{-1} is clearly invariant to polymer concentration.

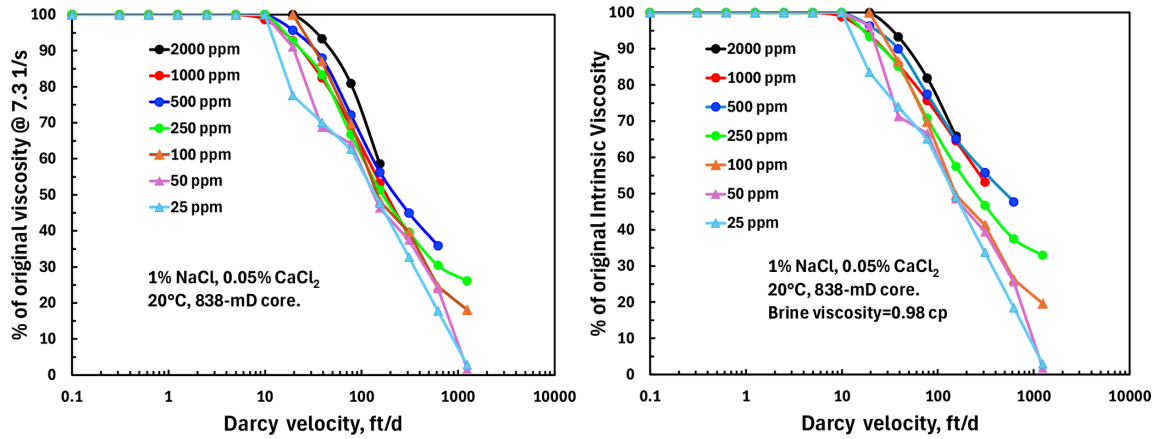

Fig. 15—HPAM mechanical degradation vs. rate and polymer concentration in the 838-md Dundee core. The percentage of remaining viscosity evaluated as $(\mu - \mu_s)/(\mu_o - \mu_s) \times 100$ (left graph) or $[\mu]/[\mu_o] \times 100$ (right graph).

However, is viscosity measured at 7.3 s^{-1} an appropriate parameter for evaluating mechanical degradation? Indeed, because of the non-Newtonian character of polymer solutions, mechanical degradation (alternatively called "extensional degradation") of a given solution depends on the shear rate at which viscosity is measured. For example, solutions at low polymer concentration or high degradation level will be on the low shear plateau, whereas solutions at high polymer concentration or low degradation will be in the shear-thinning regime. Using an intrinsic parameter representative of the polymer size, such as intrinsic viscosity $[\mu]$ or polymer Mw would be more pertinent. However, for this experiment, the viscosity of the effluent samples was measured at a single shear rate of 7.3 s^{-1}. The model of Jouenne and Levache (2020) was nevertheless used for estimating the intrinsic viscosity of all the solutions. From these estimated values, the retention of original intrinsic viscosity (expressed as $[\mu]/[\mu_o] \times 100$) is plotted in **Fig. 15**(right). The trend is the same as in **Fig. 15**(left), so there is no significant dependence of degradation on polymer concentration in the concentration range from 25 ppm to 2,000 ppm (which corresponds to $C[\mu]$ varying between 0.084 and 6.7, by taking the intrinsic viscosity of the solution determined at 3.35 L/g and assuming a solvent density of 1 g/cm3). We conclude that degradation calculated from intrinsic viscosity gives the same trend as when using viscosity measured at 7.3 s^{-1}. (If one wished to push the issue, one could argue that mechanical degradation is slightly greater at low concentrations than at high concentrations. However, the effect is small.) During future experiments, it would be interesting to evaluate mechanical degradation using intrinsic viscosity measurements obtained from low-shear viscosity plateau to confirm our conclusion.

Discussion

Onset of Shear Thickening, u_{onset}. As discussed in the "Introduction," there are several ways to define the onset of shear thickening (u_{onset}) in porous media. If the velocity at which the resistance factor is minimum (RF_{min} at u_{min}) is considered as the onset of shear thickening, **Figs. 5, 7 through 9, and 13** suggest that the onset velocity is very weakly dependent on salinity for different types of brines (NaCl/$CaCl_2$ 20/1, pure NaCl, or 1% NaCl brine with varying $CaCl_2$ concentration) or polymer concentration. If we consider that the resistance factor is the sum of two contributions, shear viscosity and shear thickening due to elastic instabilities and extensional viscosity, we can predict the resistance factor curve (resistance factor vs. Darcy velocity) as the sum of two flow curves. The shear viscosity is expressed by a Carreau model, while the elastic contribution is expressed by a Cross model, as suggested by Galindo-Rosales et al. (2011). For illustration, **Fig. 16** plots two arbitrary (dashed) flow curves. The shear-thinning region of the shear viscosity curve (the orange dashed curve) starts at 1 ft/D, while shear thickening (green dashed curve) starts at u_{onset} = 10 ft/D. Below 10 ft/D, the observed resistance factor results only from the contribution of shear viscosity. Above 10 ft/D, the observed resistance factor (solid black curve) results from the sum of the two dashed curves. For this example, the shear-thickening contribution (up to a velocity of 17 ft/D) remains small (relative to the shear-thinning contribution), so the resistance factor will continue to decrease until the velocity, u_{min} = 17 ft/D. This example points out why it might be misleading to assume that the velocity at which the resistance factor is minimum (RF_{min} at u_{min}) is the onset of shear thickening (i.e., $u_{onset} = u_{min}$).

Now, let us discuss what could trigger the onset of shear thickening in our experiments. In pure extensional flow, De Gennes (1979) predicted that coils in dilute solution will experience a sudden coil-stretch transition at a critical strain rate, $\dot{\varepsilon}_c$, that is inversely proportional to the longest relaxation time of the polymer coil.

In different geometries, McKinley et al. (1996) proposed a criterion, $M \propto \sqrt{\mathrm{WeDe}}$, for the onset of purely elastic instabilities. Both Weissenberg and Deborah numbers contain the relaxation time of the fluid.

For synthetic polymers in aqueous solution, a convenient measure of relaxation time is the relaxation time λ determined from the fitting of the flow curve (steady shear viscosity vs. shear rate) from a Carreau equation $\mu(\dot{\gamma}) = \mu_\infty + (\mu_P - \mu_\infty)\left(1 + (\lambda\dot{\gamma})^2\right)^{(n-1)/2}$, where μ is the viscosity at shear rate $\dot{\gamma}$, μ_P is the low-shear plateau viscosity, μ_∞ is the viscosity at infinite shear rate plateau viscosity, and n is the shear-thinning index. This relaxation time corresponds approximately to the inverse of the shear rate at which shear thinning starts (where polymer coils are first deformed).

This relaxation time may be pertinent for determining the onset of shear thickening. Indeed, if shear thickening is triggered by the appearance of elastic instabilities, these instabilities may appear if chains are deformed. Before the appearance of shear thickening, a flow field could be dominated by shear flow with undeformed coils. At a given velocity or shear rate in the porous medium, coils will start to be deformed—marking the beginning of the shear-thinning region. When velocity is increased further, elastic stresses grow until the

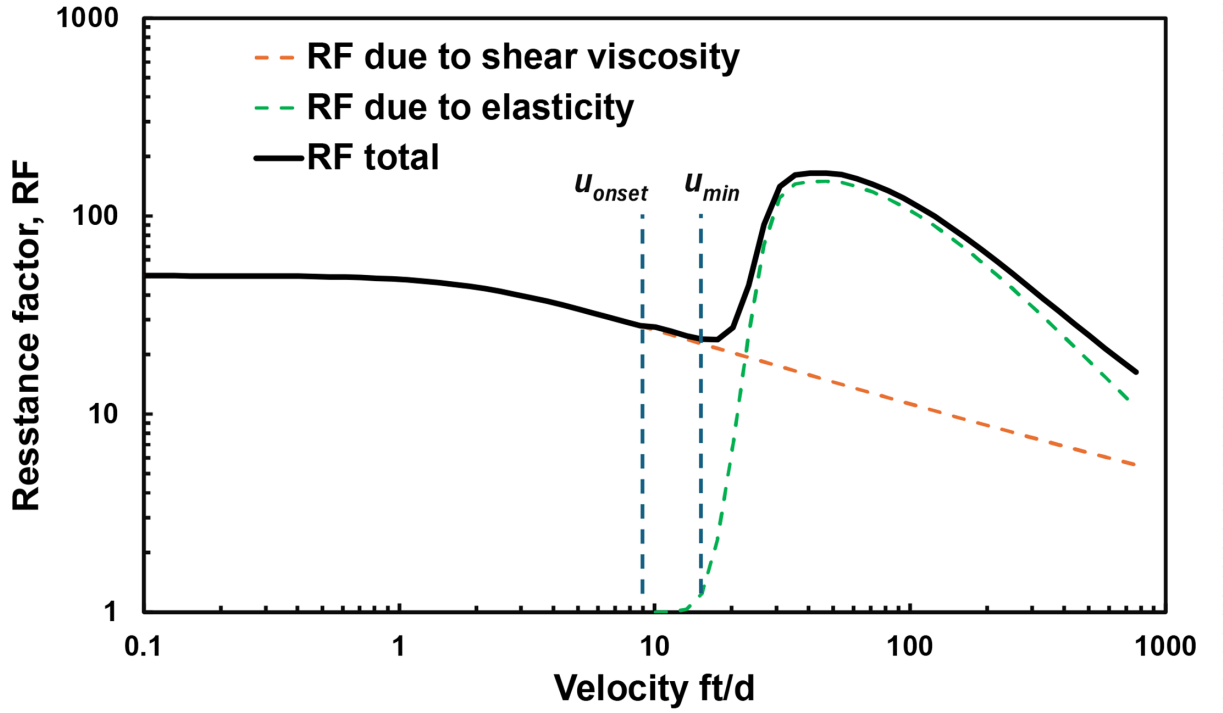

Fig. 16—Illustration of the resistance factor (black solid line) being the sum of two contributions—shear viscosity expressed by a Carreau equation (orange dashed line) and shear thickening expressed as a Cross model (green dashed line).

velocity at which elastic instabilities appear. Put in terms of cause and effect, the coil-stretch transition is the cause, and elastic instabilities may be the effect. Determining the shear rate at which coils are deformed during bulk viscosity measurement is thus quite relevant. This shear rate is approximately the inverse of the relaxation time from the Carreau equation (De Gennes 1979). In a core, the topology of the porous medium (e.g., permeability, porosity, tortuosity, connectivity, and shape of grain) determines the correspondence between shear rate in a porous medium ($\dot{\gamma}_{PM}$) and velocity u. Jouenne and Heurteux (2019) suggested a relationship of the form, $\dot{\gamma}_{PM} = \frac{1}{\beta} u$, where u is the Darcy velocity and $1/\beta$ is a geometrical factor. In practice, β is determined empirically from the shear-thickening curve by adjustment to match shear-thickening behavior for similar curves under other conditions, as described by Jouenne and Heurteux (2019).

From the steady shear rheological measurements of the polymer solution (bulk viscosity vs. shear rate), we obtain the relaxation time, λ. Polymer coils will be deformed in the porous medium when $\dot{\gamma}_{PM} > 1/\lambda$, which is equivalent to $u > \beta/\lambda$.

From this very simple analysis, we examine whether the inverse of the relaxation time can provide a good estimate of the onset of shear thickening, based on $u_{onset} = \beta/\lambda$. The model of Jouenne and Levache (2020) was used on each flow curve in Appendix A (determination of viscosity vs. shear rate in a rheometer for each polymer solution), thereby determining the intrinsic viscosity and the relaxation time of each polymer solution. We then represented the onset velocity for each resistance factor curve in this paper by a purple "x." Each "x" is calculated from the inverse of relaxation time determined from the flow curve λ multiplied by a parameter β being constant for all the resistance factor curves obtained in a porous medium. Each "x" corresponds to a resistance factor value, which was adjusted so that the "x" fell on the resistance factor curve.

As seen by the purple curves with the "x"s in **Figs. 5, 7 through 9, and 13**, the trends obtained for the calculated onset velocity seem consistent. From this analysis, we suggest that the onset velocity u_{onset} plausibly could be inversely proportional to the relaxation time of the solution determined from steady shear rheology on the bulk solution (flow curve). The values of u_{onset}, λ, $[\mu]$, and β are listed in **Table A-1** of Appendix A.

Maximum of the Resistance Factor Curve, RF_{max}. From the analysis of the resistance factor curves in **Figs. 5, 7 through 9, and 13**, it was not possible to find a parameter correlating the evolution of the velocity u_{max} at which resistance factor is maximum. As seen in **Figs. 5, 7 through 9**, u_{max} is nearly constant whatever the total salinity and ionic composition for 2,000-ppm HPAM solutions. u_{max} was around 7.8 ft/D in the 252-md Berea core and 20 ft/D in the 738-md Berea core. At low polymer concentrations (below C^*), u_{max} appears to increase when polymer concentration decreases, as seen in **Fig. 13**.

In the preceding section, we suggested that the onset of shear thickening may correspond to small deformations of polymer coils and is related to the inverse of the relaxation time of the bulk rheological curve. In other words, u_{onset} could depend on the conformation of the polymer chains at rest. Since salinity modifies this conformation, u_{onset} depends on salinity. In contrast, u_{max} clearly does not exhibit this dependence. If the maximum of a resistance factor curve corresponds to highly deformed and highly stretched polymer chains, the small dependence of u_{max} on salinity may be explained by suggesting that once stretched, chains completely forget their initial conformation. As a consequence, u_{max} may depend on the characteristics of the stretched polymer (such as polymer Mw and concentration, along with the characteristics of the flow field within the topology of the porous medium).

Concerning the dependence of the maximum of the resistance factor curve (RF_{max}), the experiments at varying polymer concentration (25–2,000 ppm) in the 838-md Dundee core indicate a linear dependence of RF_{max} with polymer concentration C, as seen in **Fig. 17**(left). When comparing solutions at various salinities, it seems pertinent to use the reduced concentration C/C^*, with C^* being the overlap concentration. Since $C^* \sim 1/[\mu]$, we have $C/C^* \sim C[\mu]$. To take into account the characteristics of the porous medium, we can use the radius of the pore R_p, estimated by the capillary bundle model as $R_p \propto (k/\phi)^{0.5}$. Comparing the RF_{max} values from **Figs. 5, 7 through 9, and 13**,

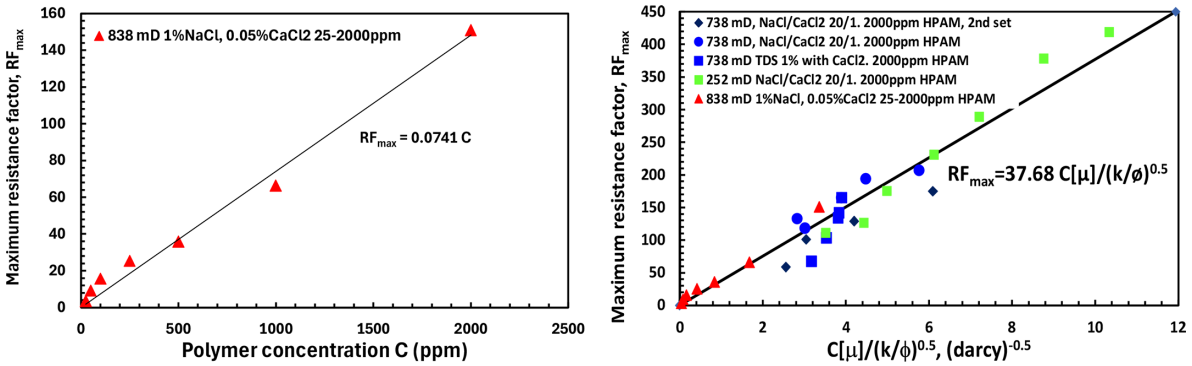

Fig. 17—(Left) Maximum resistance factor vs. polymer concentration in a 838-md Dundee core for solutions with 1% NaCl and 0.05% $CaCl_2$. (Right) Maximum resistance factor for different core permeabilities, salinities, and polymer concentrations.

we plotted RF_{max} vs. $C[\mu]/(k/\phi)^{0.5}$. As seen in **Fig. 17**(right), the maximum resistance factor in the shear-thickening regime correlated well with $C[\mu]/(k/\phi)^{0.5}$ over a broad range of conditions. These results, where $RF_{max} \propto C[\mu]/R_p$, need to be confirmed using other cores and other polymer solutions. Interestingly, there is no obvious transition in the relation at C^* (because the data in **Fig. 17** appear linear over the entire concentration range). This evidence again is consistent with the idea that at the maximum resistance factor, polymer chains are fully stretched with no impact of entanglements with other chains.

Practical Implications for Polymer Flooding. As expected, viscosity and resistance factor for HPAM solutions increased in magnitude with increased polymer concentration, increased polymer Mw, decreased salinity, and decreased divalent ion content. For a given condition, estimates of the magnitude of HPAM viscosity may be correlated/estimated using methods such as those from Jouenne and Levache (2020). However, particularly for shear-thickening behavior in porous media, projecting resistance factors at moderate-high velocities based on viscosity data alone can be challenging (Jouenne and Heurteux 2019).

A practical benefit from the current work is that it reveals that the velocity for the onset of shear-thickening behavior was only very slightly sensitive to salinity or divalent ion content. Also, as revealed in **Figs. 1 and 13**, the velocity dependence for shear thickening was only very slightly dependent on HPAM concentration, above C^*. These facts should considerably simplify modeling/simulation efforts where knowledge of the existence of shear thickening is important. Our observations concerning the relative magnitude of minimum resistance factors and maximum resistance factors in the shear-thickening regime should also be of value (i.e., **Figs. 10 and 17** and **Table A-1**). A model was proposed demonstrating that the onset of shear thickening in porous media could be correlated with the inverse of the relaxation time of the solution determined from bulk rheological measurement.

As has been known for many years (Cannella et al. 1988; Seright et al. 2011, 2023), the onset of shear thickening in porous media correlates well with the parameter, $(k\phi)^{0.5}/(1-\phi)$ (e.g., **Figs. 2 and 3**). Coupling these observations with the onset of shear thickening correlating inversely with the square of HPAM Mw (i.e., **Fig. 4**) should also be of benefit when attempting to quantify when/whether shear thickening is important during modeling/simulation of polymer floods. Incidentally, Azad and Seright (2025) performed an extensive analysis of existing field polymer floods and concluded that only a very small fraction of any given reservoir is likely to experience shear thickening during polymer injection. Nevertheless, if one insisted that vertical polymer injection wells were not fractured, the near-wellbore velocities experienced in several important existing polymer floods (Daqing, Mangala, Marmul, and Tambaredjo) are those where substantial shear thickening was noted in our work (Azad and Seright 2025).

Because of their anionic character, HPAM molecules are known to expand as salinity and hardness decrease (because of electrostatic repulsion between the anionic monomer units and because of intramolecular bridging by multivalent cations). It has also long been known (Vela et al. 1976) that HPAM molecules of a given Mw may experience difficulty penetrating into low-permeability rock (e.g., as permeability decreases below 100 md for a 20-million-dalton polymer). One might expect HPAM of a given Mw to exhibit decreasing ability to penetrate into low-permeability rock as salinity and hardness decrease but **Figs. 5 and 7 through 9** do not support this concept. In all these experiments, no evidence of rock plugging (either on the sandface or within the core) was observed as a function of polymer throughput, salinity, or calcium concentration.

Of course, our observations and correlations are most likely to apply to relatively permeable sands/sandstones (which currently account for virtually all medium- to large-scale polymer floods; Seright and Wang 2023a). Whether they are valid in low-permeability carbonates has yet to be established. Nevertheless, models that extrapolate experimental data are essential during simulations or projections of polymer flooding performance (Delshad et al. 2008; Jouenne and Levache 2020; Li et al. 2024). For that reason, our data and observations can significantly improve projections in many polymer flooding circumstances.

Conclusions

The following observations were noted for HPAM (~19 million g/mol, 30% hydrolysis) solutions in 252–838-md sandstones at 20°C:

1. Consistent with the suggestions of Chauveteau (1981) and Southwick and Manke (1988), the data from this paper support the assertion that the cause of the "shear-thickening" effect in porous media is the coil-stretch transition of individual polymer coils. Entanglements are not relevant to the explanation of shear thickening for HPAM concentrations typically used during polymer flooding.
2. As expected, the magnitude of resistance factors increased with increased HPAM concentration but decreased with increased salinity (NaCl and $CaCl_2$ concentration).
3. The maximum resistance factor in the shear-thickening regime correlated well with $C[\mu]/(k/\phi)^{0.5}$ over a broad range of conditions.
4. The velocity dependence of the rheology was very slightly dependent on salinity between 0.1% and 5% TDS.
5. At 1% TDS, the velocity dependence of rheology was largely unaffected by $CaCl_2$ concentration between 0 ppm and 1,000 ppm.
6. With a salinity of 1% NaCl and 0.05% $CaCl_2$, the velocity dependence of shear thickening was very slightly affected by HPAM concentration, especially between 250 ppm and 2,000 ppm.

7. The entrance pressure drop exhibited by HPAM solutions at high velocities did not correlate with either salinity or $CaCl_2$ content.
8. Confirming previous literature reports, HPAM mechanical degradation increased with increased salinity and $CaCl_2$ content.
9. Mechanical degradation of HPAM was not strongly dependent on polymer concentration between 25 ppm and 2,000 ppm (in brine with 1% NaCl and 0.05% $CaCl_2$).
10. An analysis combined rheological measurements in bulk and porous media to project the onset of shear thickening. For all the conditions examined (i.e., polymer concentrations, salinities, Na/Ca ratios, and rock permeabilities), the onset of shear thickening could be viewed as proportional to the inverse of the relaxation time determined from the bulk steady shear viscosity curve (viscosity vs. shear rate).

Nomenclature

C = polymer concentration, ppm
C^* = overlap concentration, ppm
C/C^* = reduced concentration
C_e = entanglement concentration, ppm
$C[\mu]$ = overlap concentration
De = Deborah number
G' = elastic modulus, psi [Pa]
G'' = loss modulus, psi [Pa]
k = permeability, darcies [μm^2]
k_{rw} = relative permeability to water at residual oil saturation, darcies [μm^2]
k_w = permeability to water at residual oil saturation, darcies [μm^2]
M_w = polymer molecular weight, g/mol [daltons]
n = shear-thinning index
RF_{max} = maximum resistance factor in the shear-thickening region
RF_{min} = minimum resistance factor just before the shear-thickening region
R_p = pore radius in the capillary bundle model, μm
S_{or} = resident oil saturation
Sp = exponent for power-law equation in Fig. 6
TDS = total dissolved solids, wt%
u = Darcy velocity, ft/D [cm/s]
u_{max} = velocity associated with the maximum in the resistance factor vs. velocity curve, ft/(D-md$^{0.5}$) or ft/D [cm/s]
u_{min} = velocity associated with the minimum in the resistance factor vs. velocity curve, ft/(D-md$^{0.5}$) or ft/D [cm/s]
u_{onset} = velocity associated with the onset of shear thickening, ft/(D-md$^{0.5}$) or ft/D [cm/s]
We = Weissenberg number
β = "geometric parameter" associated with discussion of Fig. 16
$\dot{\gamma}$ = shear rate, s^{-1}
$\dot{\gamma}_{PM}$ = shear rate in a porous medium, s^{-1}
$\dot{\varepsilon}_c$ = critical strain rate, s^{-1}
λ = relaxation time of the polymer solution, seconds
μ = viscosity, cp [mPa·s]
μ_o = original viscosity before injection, cp [mPa·s]
μ_p = polymer plateau viscosity at very low shear rates in the Carreau model, cp [mPa·s]
μ_s = solvent viscosity, cp [mPa·s]
μ_∞ = polymer plateau viscosity at very high shear rates in the Carreau model, cp [mPa·s]
$[\mu]$ = intrinsic viscosity, L/g [m^3/kg]
ϕ = porosity

Acknowledgment

The authors are grateful to Professor François Lequeux, ESPCI, Paris, for interesting discussion about shear thickening in porous medium and his suggestion to plot the onset velocities predicted from the relaxation time of bulk rheology directly on the resistance factor curves.

References

AlAbdullah, M. B., Seright, R. S., Machado, M. V. B. et al. 2023. An Analytical Tool to Predict Fracture Extension and Elastic Desaturation for Polymer Field Projects. Paper presented at the SPE Annual Technical Conference and Exhibition, San Antonio, Texas, USA, 16−18 October. https://doi.org/10.2118/215083-MS.

Alfazazi, U., Chacko Thomas, N., Al-Shalabi, E. W. et al. 2021. Investigation of Oil Presence and Wettability Restoration Effects on Sulfonated Polymer Retention in Carbonates Under Harsh Conditions. Paper presented at the Abu Dhabi International Petroleum Exhibition & Conference, Abu Dhabi, UAE, 15−18 November. https://doi.org/10.2118/207892-MS.

Azad, M. S. 2023. Characterization of Nonlinear Viscoelastic Properties of Enhanced Oil Recovery Polymer Systems Using Steady-Shear Rheometry. *SPE J.* **28** (02): 664–682. https://doi.org/10.2118/212824-PA.

Azad, M. and Seright, R. S. 2025. Are Field Polymer EOR Projects Reaping the Benefits of SOR Reduction Due to Polymer Viscoelasticity. *SPE J*. **28**. https://doi.org/10.2118/223155-PA.

Azad, M.S. and Trivedi, J. J. 2019. Novel Viscoelastic Model for Predicting the Synthetic Polymer's Viscoelastic Behavior in Porous Media Using Direct Extensional Rheological Measurements. *Fuel* **235**: 218–226. https://doi.org/10.1016/j.fuel.2018.06.030.

Azad, M. S. and Trivedi, J. J. 2020a. Does Polymer's Viscoelasticity Influence Heavy-Oil Sweep Efficiency and Injectivity at 1 ft/D? *SPE Res Eval & Eng* **23** (02): 446–462. https://doi.org/10.2118/193771-PA.

Azad, M. S. and Trivedi, J. J. 2020b. Quantification of *Sor* Reduction during Polymer Flooding Using Extensional Capillary Number. *SPE J.* **26** (3): 1469–1498. https://doi.org/10.2118/204212-PA.

Briscoe, B., Luckham, P., and Zhu, S. 1999. Pressure Influences upon Shear Thickening of Poly(Acrylamide) Solutions. *Rheologica Acta* **38** (3): 224–234. https://doi.org/10.1007/s003970050172.

Cannella, W. J., Huh, C., and Seright, R. S. 1988. Prediction of Xanthan Rheology in Porous Media. Paper presented at the SPE Annual Technical Conference and Exhibition, Houston, Texas, USA, 2−5 October. https://doi.org/10.2118/18089-MS.

Casanellas, L., Alves, M. A., Poole, R. J. et al. 2016. The Stabilizing Effect of Shear Thinning on the Onset of Purely Elastic Instabilities in Serpentine Microflows. *Soft Matter* **12** (29): 6167–6175. https://doi.org/10.1039/c6sm00326e.

Chauveteau, G. 1981. Molecular Interpretation of Several Different Properties of Flow of Coiled Polymer Solutions Through Porous Media in Oil Recovery Conditions. Paper presented at the SPE Annual Technical Conference and Exhibition, San Antonio, Texas, USA, 4−7 October. https://doi.org/10.2118/10060-MS.

Chauveteau, G. and Moan, M. 1981. The Onset of Dilatant Behaviour in Non-Inertial Flow of Dilute Polymer Solutions through Channels with Varying Cross-Sections. *J Phyique Lett* **42** (10): 201–204. https://doi.org/10.1051/jphyslet:019810042010020100.

Chen, E. Y. and Datta, S. S. 2024. Influence of Fluid Rheology on Multistability in the Unstable Flow of Polymer Solutions through Pore Constriction Arrays. arXiv:2407.00778 (preprint; submitted on 30 June 2024). https://doi.org/10.48550/arXiv.2407.00778.

Clarke, A., Howe, A. M., Mitchell, J. et al. 2016. How Viscoelastic-Polymer Flooding Enhances Displacement Efficiency. *SPE J.* **21** (03): 0675–0687. https://doi.org/10.2118/174654-PA.

Colby, R. H. 2010. Structure and Linear Viscoelasticity of Flexible Polymer Solutions: Comparison of Polyelectrolyte and Neutral Polymer Solutions. *Rheol Acta* **49** (5): 425–442. https://doi.org/10.1007/s00397-009-0413-5.

De Gennes, P.-G. 1979. *Scaling Concepts in Polymer Physics*. Ithaca: Cornell University Press.

Delshad, M., Kim, D. H., Magbagbeola, O. A. et al. 2008. Mechanistic Interpretation and Utilization of Viscoelastic Behavior of Polymer Solutions for Improved Polymer-Flood Efficiency. Paper presented at the SPE Symposium on Improved Oil Recovery, Tulsa, Oklahoma, USA, 20−23 April. https://doi.org/10.2118/113620-MS.

Durst, F., Haas, R., and Interthal, W. 1982. Laminar and Turbulent Flows of Dilute Polymer Solutions: A Physical Model. *Rheol Acta* **21** (4–5): 572–577. https://doi.org/10.1007/BF01534350.

Ekanem, E. M., Berg, S., De, S. et al. 2022. Towards Predicting the Onset of Elastic Turbulence in Complex Geometries. *Transp Porous Med* **143** (1): 151–168. https://doi.org/10.1007/s11242-022-01790-8.

Galindo-Rosales, F. J., Rubio-Hernández, F. J., Sevilla, A. et al. 2011. How Dr. Malcom M. Cross May Have Tackled the Development of "An Apparent Viscosity Function for Shear Thickening Fluids". *J Nonnewton Fluid Mech* **166** (23–24): 1421–1424. https://doi.org/10.1016/j.jnnfm.2011.08.008.

Garrepally, S., Jouenne, S., Leuqeux, F. et al. 2020. Polymer Flooding - Towards a Better Control of Polymer Mechanical Degradation at the Near Wellbore. Paper presented at the SPE Improved Oil Recovery Conference, Virtual, 31 August−4 September. https://doi.org/10.2118/200373-MS.

Garrepally, S., Jouenne, S., Olmsted, P. D. et al. 2023. Scission of Flexible Polymers in Contraction Flow: Predicting the Effects of Multiple Passages. *J Rheol* **64** (3): 601–614. https://doi.org/10.1122/1.5127801.

Gumpenberger, T., Deckers, M., Kornberger, M. et al. 2012. Experiments and Simulation of the Near-Wellbore Dynamics and Displacement Efficiencies of Polymer Injection, Matzen Field, Austria. Paper presented at the Abu Dhabi International Petroleum Conference and Exhibition, Abu Dhabi, UAE, 11−14 November. https://doi.org/10.2118/161029-MS.

Heemskerk, J., Janssen-van Rosmalen, R., Holtslag, R. J. et al. 1984. Quantification of Viscoelastic Effects of Polyacrylamide Solutions. Paper presented at the SPE Enhanced Oil Recovery Symposium, Tulsa, Oklahoma, USA, 15−18 April. https://doi.org/10.2118/12652-MS.

Hirasaki, G. J. and Pope, G. A. 1974. Analysis of Factors Influencing Mobility and Adsorption in the Flow of Polymer Solution Through Porous Media. *SPE J.* **14** (04): 337–346. https://doi.org/10.2118/4026-PA.

Howe, A. M., Clarke, A., and Giernalczyk, D. 2015. Flow of Concentrated Viscoelastic Polymer Solutions in Porous Media: Effect of M_W and Concentration on Elastic Turbulence Onset in Various Geometries . *Soft Matter* **11** (32): 6419–6431. https://doi.org/10.1039/C5SM01042J.

Hwang, J., Zheng, S., Sharma, M. et al. 2022. Use of Horizontal Injectors for Improving Injectivity and Conformance in Polymer Floods. Paper presented at the SPE Improved Oil Recovery Conference, Virtual, 25−29 April. https://doi.org/10.2118/209373-MS.

Jouenne, S. and Levache, B. 2020. Universal Viscosifying Behavior of Acrylamide-Based Polymers Used in Enhanced Oil Recovery. *J Rheol* **64** (5): 1295–1313. https://doi.org/0148-6055/2020/54(5)/1295/19.

Khodaverdian, M., Sorop, T., Postif, S. et al. 2010. Polymer Flooding in Unconsolidated-Sand Formations: Fracturing and Geomechanical Considerations. *SPE Prod & Oper* **25** (02): 211–222. https://doi.org/10.2118/121840-PA.

Li, Z., Dean, R. M., Lashgari, H. et al. 2024. Recent Advances in Modeling Polymer Flooding. Paper presented at the SPE Improved Oil Recovery Conference, Tulsa, Oklahoma, USA, 22−25 April. https://doi.org/10.2118/218219-MS.

Jennings, R. R., Rogers, J. H., and West, T. J. 1971. Factors Influencing Mobility Control By Polymer Solutions. *J Pet Tech* **23** (03): 391–401. https://doi.org/10.2118/2867-PA.

Jouenne, S., Chakibi, H., and Levitt, D. 2018. Polymer Stability After Successive Mechanical-Degradation Events. *SPE J.* **23** (01): 18–33. https://doi.org/10.2118/186103-PA.

Jouenne, S. and Heurteux, G. 2019. Correlation of Mobility Reduction of HPAM Solutions at High Velocity in Porous Medium with Ex-Situ Measurements of Elasticity. *SPE J.* **25** (01): 465–480. https://doi.org/10.2118/198899-PA.

Li, Z., Espinoza, D. N., and Balhoff, M. T. 2023. Simulation of Polymer Injection in Granular Media: Implications of Fluid-Driven Fractures, Water Quality, and Undissolved Polymers on Polymer Injectivity. *SPE J.* **28** (01): 289–300. https://doi.org/10.2118/200412-PA.

Lohne, A., Nødland, O., Stavland, A. et al. 2017. A Model for Non-Newtonian Flow in Porous Media at Different Flow Regimes. *Comput Geosci* **21** (5–6): 1289–1312. https://doi.org/10.1007/s10596-017-9692-6.

Ma, Y. and McClure, M. W. 2017. The Effect of Polymer Rheology and Induced Fracturing on Injectivity and Pressure-Transient Behavior. *SPE Res Eval & Eng* **20** (02): 394–402. https://doi.org/10.2118/184389-PA.

Maerker, J. M. 1975. Shear Degradation of Partially Hydrolyzed Polyacrylamide Solutions. *SPE J.* **15** (04): 311–322. https://doi.org/10.2118/5101-PA.

Masalmeh, S., AlSumaiti, A., Gaillard, N. et al. 2019. Extending Polymer Flooding Towards High-Temperature and High-Salinity Carbonate Reservoirs. Paper presented at the Abu Dhabi International Petroleum Exhibition & Conference, Abu Dhabi, UAE, 11−14 November. https://doi.org/10.2118/197647-MS.

Masuda, Y., Tang, K.-C., Miyazawa, M. et al. 1992. 1D Simulation of Polymer Flooding Including the Viscoelastic Effect of Polymer Solution. *SPE Res Eng* **7** (02): 247–252. https://doi.org/10.2118/19499-PA.

McKinley, G. H., Pakdel, P., and Öztekin, A. 1996. Rheological and Geometric Scaling of Purely Elastic Flow Instabilities. *J Nonnewton Fluid Mech* **67**: 19–47. https://doi.org/10.1016/S0377-0257(96)01453-X.

Nguyen, T. Q. and Kausch, H. H. 1990. Effects of Solvent Viscosity on Polystyrene Degradation in Transient Elongational Flow. *Macromolecules* **23** (24): 5137–5145. https://doi.org/10.1021/ma00226a017.

Rock, A., Hincapie, R. E., Tahir, M. et al. 2020. On the Role of Polymer Viscoelasticity in Enhanced Oil Recovery: Extensive Laboratory Data and Review. *Polym* **12**: 2276. https://doi.org/10.3390/polym12102276.

Sagyndikov, M., Seright, R., Kudaibergenov, S. et al. 2022. Field Demonstration of the Impact of Fractures on Hydrolyzed Polyacrylamide Injectivity, Propagation, and Degradation. *SPE J.* **27** (02): 999–1016. https://doi.org/10.2118/208611-PA.

Sasmal, C. 2023. Applications of Elastic Instability and Elastic Turbulence: Review, Limitations, and Future Directions arXiv:2301.02395 (preprint; submitted on 6 January 2023). https://doi.org/10.48550/arXiv.2301.02395.

Seright, R. S. 1983. The Effects of Mechanical Degradation and Viscoelastic Behavior on Injectivity of Polyacrylamide Solutions. *SPE J.* **23** (03): 475–485. https://doi.org/10.2118/9297-PA.

Seright, R. S. 1991. Effect of Rheology on Gel Placement. *SPE Res Eng* **6** (02): 212–218. https://doi.org/10.2118/18502-PA.

Seright, R. S. 2009. Use of Polymers to Recover Viscous Oil from Unconventional Reservoirs. First Annual Report. United States Department of Energy. DOE Award No. DE-NT0006555.

Seright, R. S. 2017. How Much Polymer Should Be Injected During a Polymer Flood? Review of Previous and Current Practices. *SPE J.* **22** (01): 1–18. https://doi.org/10.2118/179543-PA.

Seright, R. S., Maerker, J. M., and Holzwarth, G. M. 1981. Mechanical Degradation of Polyacrylamides Induced by Flow Through Porous Media. *Am Chem Soc Polym Prepr* **22**: 30–33.

Seright, R. S., Seheult, M., and Talashek, T. 2009. Injectivity Characteristics of EOR Polymers. *SPE Res Eval & Eng* **12** (5): 783–792. https://doi.org/10.2118/115142-PA.

Seright, R.S. and Wang, D. 2023a. Polymer Flooding: Current Status and Future Directions. *Pet Sci* **20** (2): 910–921. https://doi.org/10.1016/j.petsci.2023.02.002.

Seright, R. S., Azad, M. S., AlAbdullah, M. B. et al. 2023. Effect of Residual Oil Saturation and Salinity on HPAM Rheology in Porous Media. Paper presented at the SPE Annual Technical Conference and Exhibition, San Antonio, Texas, USA, 16−18 October. https://doi.org/10.2118/215060-MS.

Seright, R. S. . S., Fan, T., Wavrik, K. et al. 2011. New Insights Into Polymer Rheology in Porous Media. *SPE J.* **16** (01): 35–42. https://doi.org/10.2118/129200-PA.

Seright, R. S., Jouenne, S., and Aften, C. 2025. Effect of Salinity and Hardness on HPAM Rheology in Sandstone. Paper presented at the SPE International Conference on Oilfield Chemistry, Galveston, Texas, USA, 9−10 April. https://doi.org/10.2118/224231-MS.

Seright, R. and Wang, D. 2023b. Literature Review and Experimental Observations of the Effects of Salinity, Hardness, Lithology, and ATBS Content on HPAM Polymer Retention for the Milne Point Polymer Flood. *SPE J.* **28** (5): 2300–2315. https://doi.org/10.2118/212946-PA.

Seright, R. S., Wavrik, K. E., Zhang, G. et al. 2021. Stability and Behavior in Carbonate Cores for New Enhanced-Oil-Recovery Polymers at Elevated Temperatures in Hard Saline Brines. *SPE Res Eval & Eng* **24** (01): 1–18. https://doi.org/10.2118/200324-PA.

Skauge, A., Zamani, N., Gausdal Jacobsen, J. et al. 2018. Polymer Flow in Porous Media: Relevance to Enhanced Oil Recovery. *Colloid Interface* **2** (3): 27. https://doi.org/10.3390/colloids2030027.

Southwick, J. G. and Manke, C. W. 1988. Molecular Degradation, Injectivity, and Elastic Properties of Polymer Solutions. *SPE Res Eng* **3** (4): 1193–1201. https://doi.org/10.2118/15652-PA.

Vela, S., Peaceman, D. W., and Sandvik, E. I. 1976. Evaluation of Polymer Flooding in a Layered Reservoir With Crossflow, Retention, and Degradation. *SPE J.* **16** (02): 82–96. https://doi.org/10.2118/5102-PA.

Wang, D., Li, C., and Seright, R. S. 2020. Laboratory Evaluation of Polymer Retention in a Heavy Oil Sand for a Polymer Flooding Application on Alaska's North Slope. *SPE J.* **25** (04): 1842–1856. https://doi.org/10.2118/200428-PA.

Willhite, G. P. and Uhl, J. T. 1988. Correlation of the Flow of Flocon 4800 Biopolymer with Polymer Concentration and Rock Properties in Berea Sandstone. In *Water-Soluble Polymers for Petroleum Recovery*, eds. G. A. Stahl and D. N. Schulz, 101–119. Boston, Massachusetts, USA: Springer. https://doi.org/10.1007/978-1-4757-1985-7_5.

Yin, G., Nakamura, Y., Suzuki, H. et al. 2024. Memory and Scission Effects of Polymers on the Flow Regime of Polyethylene Oxide Solutions in Continuous Abrupt Contraction–Expansion Microchannels with Different Cavity Lengths. *Phys Fluids (1994)* **36** (4). https://doi.org/10.1063/5.0201870.

Yuan, M. 1981. *A Rheological Study of Polymer and Microemulsion in Porous Media*. MS Thesis, University of Texas at Austin, Texas, USA.

Zaitoun, A., Makakou, P., Blin, N. et al. 2012. Shear Stability of EOR Polymers. *SPE J.* **17** (2): 335–339. https://doi.org/10.2118/141113-PA.

Zeynalli, M., Al-Shalabi, E. W., and AlAmeri, W. 2023. An Extended Unified Viscoelastic Model for Predicting Polymer Apparent Viscosity at Different Shear Rates. *SPE Res Eval & Eng* **26** (1): 99–121. https://doi.org/10.2118/206010-PA.

Appendix A—Resistance Factors and Velocities at the Minimum and Maximum Resistance Factor Values, Calculated Onset Velocity, Relaxation Time and Intrinsic Viscosity

Fig.	k (md)	(%)	C (ppm)	NaCl (ppm)	$CaCl_2$ (ppm)	u_{min} (ft/D)	RF_{min}	u_{max} (ft/D)	RF_{max}	RF_{max}/RF_{min}	(seconds)	β	$u_{onset} = \beta/\lambda$ (ft/D)	RF_{onset}	$[\mu]$ (L/g)	$C[\mu]/(k/\phi)^{0.5}$
7	738	0.21	2,000	1,000	50	0.83	80	28	175	2.2	1.69	0.60	0.35	95.0	5.71	193
	738		2,000	5,000	250	0.83	28.3	23	129	4.6	0.95		0.63	29.0	3.94	133
	738		2,000	10,000	500	0.95	20	17	101	5.1	0.76		0.79	20.0	2.86	96
	738		2,000	50,000	2,500	1.5	12	18	58.6	4.9	0.49		1.23	12.1	2.40	81
8	738	0.21	2,000	1,000	0	0.8	94	24	207	2.2	1.08	0.60	0.56	97.0	5.40	182
	738		2,000	5,000	0	0.7	29.3	24	194	6.6	1.02		0.59	40.0	4.20	142
	738		2,000	10,000	0	0.95	26.5	22	165	6.2	0.88		0.68	27.1	3.65	123
	738		2,000	50,000	0	0.95	18.6	13	118.5	6.4	0.64		0.94	21.3	2.82	95
	738		2,000	100,000	0	0.9	21.5	11	133	6.2	0.57		1.05	18.5	2.65	89

Table A-1—

Fig.	k (md)	(%)	C (ppm)	NaCl (ppm)	$CaCl_2$ (ppm)	u_{min} (ft/D)	RF_{min}	u_{max} (ft/D)	RF_{max}	RF_{max}/RF_{min}	(seconds)	β	$u_{onset} = \beta/\lambda$ (ft/D)	RF_{onset}	$[\mu]$ (L/g)	$C[\mu]/(k/\phi)^{0.5}$
9	738	0.21	2,000	10,000	0	0.95	26.5	22	165	6.2	0.95	0.60	0.63	30.5	3.66	123
	738		2,000	9,920	80	0.9	30	23	142	4.7	0.81		0.74	27.5	3.60	121
	738		2,000	9,800	200	0.7	27.3	17	134	4.9	0.78		0.77	26.5	3.57	121
	738		2,000	9,524	476	1	22.9	16	103.5	4.5	0.62		0.97	23.0	3.31	112
	738		2,000	9,000	1,000	1.243	15.6	19.9	67.3	4.3	0.59		1.02	15.7	2.97	100
5	252	0.2	2,000	1,000	50	0.466	192.4	7.77	418.6	2.2	1.60	0.30	0.19	225.0	5.66	327
	252		2,000	2,000	100	0.466	128.4	7.77	378.2	2.9	1.20		0.25	135.0	4.80	277
	252		2,000	5,000	250	0.466	72.7	7.77	289.1	4	0.95		0.31	76.0	3.95	228
	252		2,000	10,000	500	0.466	49.9	7.77	230.8	4.6	0.76		0.39	51.0	3.35	194
	252		2,000	20,000	1,000	0.466	43.4	7.77	175.4	4	0.47		0.63	43.0	2.73	158
	252		2,000	50,000	2,500	0.466	37.8	7.77	126.6	3.3	0.45		0.67	38.0	2.43	140
	252		2,000	100,000	5,000	1.3	29	11	111	3.8	0.31		0.97	28.5	1.93	111
17	838	0.21	25	10,000	500	0.62	1.22	77.7	3.49	2.9	0.16	0.20	1.28	1.2	3.35	1
	838		50	10,000	500	0.62	1.22	38.8	9.22	7.6	0.16		1.28	1.2	3.35	3
	838		100	10,000	500	0.62	1.46	38.8	15.7	10.7	0.16		1.28	1.5	3.35	5
	838		250	10,000	500	0.62	1.95	19.4	25.4	13	0.16		1.25	2.2	3.35	13
	838		500	10,000	500	1.24	4.88	19.4	35.9	7.4	0.18		1.13	5.0	3.35	27
	838		1,000	10,000	500	1.24	10.3	19.4	66.3	6.5	0.27		0.74	10.8	3.35	53
	838		2,000	10,000	500	1.24	33	19.4	151	4.6	0.76		0.26	48.0	3.35	106

Table A-1 (continued)—

SI Metric Conversion Factors	
cp×1.0*	E-03 = Pa·s
ft×3.048*	E-01 = m
in.×2.54*	E+00 = cm
md×9.869 233	E-04 = mm^2
psi×6.894 757	E+00 = kPa

* Conversion is exact.